Journal of Biological Systems, Vol. 28, No. 2 (2020) 377–429

DOI: 10.1142/S0218339020400069

World Scientific
www.worldscientific.com

A MATHEMATICAL STUDY OF THE IMPLICIT ROLE OF INNATE AND ADAPTIVE IMMUNE RESPONSES ON WITHIN-HUMAN *PLASMODIUM FALCIPARUM* PARASITE LEVELS

GIDEON A. NGWA[†], WOLDEGEBRIEL A. WOLDEGERIMA[†,‡,§] and MIRANDA I. TEBOH-EWUNGKEM[*,¶]

[*]*Department of Mathematics, Lehigh University*
Bethlehem, PA 18015, USA

[†]*Department of Mathematics, University of Buea*
P. O. Box 63, Buea, Cameroon

[‡]*African Institute for the Mathematical Sciences (AIMS) Cameroon*
P. O. Box 608, Limbe, Cameroon

[§]*CNCS, Department of Mathematics, Mekelle University*
P. O. Box 231, Tigray, Ethiopia
[¶]*ewungkems@gmail.com; [¶]mit703@lehigh.edu*

Received 15 August 2019
Accepted 19 April 2020
Published 24 June 2020

A within-human-host malaria parasite model, integrating key variables that influence parasite evolution-progression-advancement, under innate and adaptive immune responses, is analyzed. The implicit role of immunity on the steady state parasite loads and parasitemia reproduction number ($\mathscr{R}_0$), a threshold parameter measuring the parasite's annexing ability of healthy red blood cells (HRBCs), eventually rendering a human infectious to mosquitoes, is investigated. The impact of the type of recruitment function used to model HRBC growth is also investigated. The model steady states and $\mathscr{R}_0$, both obtained as functions of immune system variables, are analyzed at snapshots of immune sizes. Model results indicate that the more the immune cells, innate and adaptive, the more efficient they are at inhibiting parasite development and progression; consequently, the less severe the malaria disease in a patient. Our analysis also illustrates the existence of a Hopf bifurcation leading to a limit cycle, observable only for the *nonlinear* recruitment functions, at reasonably large $\mathscr{R}_0$.

Keywords: Malaria Parasite; Innate and Acquired Immunity; Parasitemia Reproduction Number; Gametocytes; Global Stability; Hopf Bifurcation and Limit Cycle; Anemia.

1. Introduction and Background

The WHO 2018 malaria report shows that the global malaria control progress observed a few years back, seems to be stalling.[1] Past gains achieved in the reduction of the number of global malaria cases were reversed with an estimated 219 million

[¶]Corresponding author.

cases reported in 2017, an increase by an estimated 2 million cases when compared to the year 2016.[1] The number of deaths between the two years were not that different, with an estimated 435,000 reported deaths in 2017, a slight decrease by about 16,000 from the reported 2016 estimate.[1] Of the 2017 malaria-related deaths, 61% were of children under age five. We note, however, that when compared to the 2010 statistics, the number of cases and deaths have reduced. With the report that no significant progress was made in reducing the global malaria cases between 2015 and 2017,[1] and knowing the impact that the malaria disease has on individuals, rendering them sick, leaving children febrile and weakened with a higher mortality rate among them and the impact on the economies of endemic regions, malaria research and funding needs to be intensified. Moreover, control efforts and studies aimed at understanding every facet of the disease must also intensify and mathematics has a role in this.

The agents that cause malaria are the *Plasmodium* parasites, the most deadly being *Plasmodium falciparum*, which was responsible for 99.7% of the 2017 malaria cases.[1] Parasites interact synergistically with mosquitoes, with the female *Anopheles* mosquitoes the transmitters of the parasites from one human to another. As part of their success scheme, the parasites make use of the feeding and reproductive habits of the female mosquitoes, a process necessitating a successful interaction with humans. The parasite's success and impact, especially *P. falciparum*, dates as far back at 1324 BC[2] and likely beyond. It warrants that the parasite complete a complex life-cycle with part residing in a human and the other part in the mosquito.

The within-human part of the parasite's life-cycle involves asexual reproduction associated with merozoite production. Some of the merozoites will continue the merozoite production cycle, while a smaller percentage will continue the path toward gametocytogenesis, leading to the production of parasite forms called gametocytes that may render the human infectious to mosquitoes.[3–7] A successful ingestion of mature gametocytes by a reproducing female mosquito commences the within-mosquito parts of the complex life-cycle.[3,4,8] This involves sexual reproduction, where fertilization takes place between male and female gametes generated from male and female gametocytes, respectively, with the possibility of gene recombination in the mosquito vector.[3,5,8–11] Successful fertilization produces zygotes culminating with sporozoite production that then migrate to the mosquito's salivary glands, waiting to be injected into a human during the next blood meal.

Several mathematical models aimed at understanding the various facets of the malaria transmission problem have been suggested. Some of the models have focused on the macroscopic aspects of transmission capturing the interaction between humans and vectors, see Refs. 12–17 and the many references therein. Others have focused on the mosquitoes, the agents responsible for the transmission of the parasites between humans and mosquitoes, see, for examples, Refs. 18–20 and the references therein. Yet again, others have focused on the parasite within the

mosquito,[9–11,21,22] or within the human, see Refs. 23–29 and the references there in. A recent aspect is in the coupling of the within-host dynamics to the transmission dynamics where by a within-human parasite model is linked to a macroscopic transmission model.[30] These models, a sample of the vast literature published, have extended our knowledge on malaria.

In this paper, our focus is on the within-human stages of the *P. falciparum* parasites. There are three main stages of the within-human part of *P. falciparum* life-cycle[3,4]: the exo-erythrocytic or pre-erythrocytic (this is the liver stage); the erythrocytic asexual stage (this is the merozoite or blood stage) and the erythrocyte sexual stage (this is the gametocyte blood stage). The liver stage commences when an infected blood feeding female anopheles mosquito succeeds in injecting sporozoites into a human which are transported to the human's liver by circulating blood.[5] When the sporozoites reach the liver, they infect the liver cells, multiply and develop into parasite forms called schizonts (hepatic schizonts), which upon rupture will release loads of freely floating merozoites into the bloodstream. The asexual blood stage then commences when these freely floating merozoites come in contact with *Healthy Red Blood Cells* (acronymed HRBCs), infecting them and rendering the HRBCs *infected red blood cells* (acronymed IRBCs) upon a successful interaction. The merozoites in the IRBCs undergo asexual replication with some of them rupturing to continue the cyclical pattern in which merozoites infect HRBCs and the IRBCs rupturing to produce more merozoites. This rupturing of infected red blood cells contributes to malaria related anaemia,[31] which imposes additional risks and economic burden on the malaria patient. The IRBCs that do not continue the cyclical path, instead continue toward the formation of gametocytes, the transmissible forms of the parasites to mosquitoes.[32,33] Within the human, the parasite's invasion of the RBCs and its interaction and dynamics with and within the RBCs, breaking the RBCs down and rendering the human sick, invokes the humans' natural defense mechanisms (the innate immune system). For humans who have lived long in an endemic region and have been continuously re-exposed to the malaria parasite, the process will also function in the presence of the adaptive immune system,[34–40] acquired due to the sustained exposure to the malaria parasite.

Our primary objective in this paper is to analyze the within-human host model for the *P. falciparum* malaria under implicit immune action, innate and adaptive. The model was originally developed in Ref. 29, but analyzed in the absence of these immune effectors. The model proposed in Ref. 29 accounted for gametocytes in their early and late states, typically not considered in most models, a list which includes the cited papers in the previous paragraph. However, the early state gametocytes are the precursors of late state gametocytes, with the latter, the primary link to mosquito transmission and hence vital to the continuous transmission dynamics of the parasite from humans to mosquitoes. Here, we analyze the model originally proposed in Ref. 29 under the implicit role of immune effectors. The analyses will be carried out for different proposed HRBC production functions. HRBCs are vital

to every human but also to the malaria parasite. In an infected human, gametocytes are transmitted from humans to mosquitoes within an infected red blood cell. If the parasites (in this case merozoites) cannot infect HRBCs then it is likely that the parasite-cycle within the human can be terminated. The fewer red blood cells there are to infect, which in this case the human is highly anemic, the lower the parasite load. Thus, the reduction in HRBC population in a human, especially an immunologically naive human, is related to malaria intensity, and severity and the relation is affected by the human's adaptive immune response. Thus, it is important to understand this relationship. It is, of course, important to understand how HRBCs are formed and maintained in a healthy human or infected human. However, as a first step in this process, we will make some simplifying assumptions and not focus on the generation from the stem cell. Hence, we will evoke different linear and nonlinear types of recruitment functions for the HRBC population and derive bounds for the different parasite and immune cell types studied as functions of bounds of the recruitment functions. This, in some sense, generalizes past works where either a constant or a linear recruitment function for HRBC production in humans was used, for the purpose of mathematical tractability (see, for example, Refs. 25, 30, 41 and 28). We believe that our model can provide some mathematical insights into the relationship between parasite loads under immune protection for various recruitment functions in humans and for *P. falciparum* malaria.

A second objective of this study is to ascertain how the presence of immunity can mitigate the growth of the parasite within a human for the various HRBC recruitment functions. To this effect, we view the immune presence as parameters of the system variables and study how these immunity-based variables will affect the size and intensity of the infection in the human body. We believe this is appropriate since adaptive immunity to malaria is still not very well understood. Moreover, the adaptive immune response dynamics is highly variable within each human, especially across age groups. Our general motivation lies in the quest, through the use of mathematics, to better understand malaria as a disease in human populations and also to address the interesting mathematical aspects arising from the modeling exercise.

The rest of the paper is organized as follows: in Sec. 2, we present the model equations to be studied and discuss on the nature of recruitment functions used. We invoke the basic mathematical properties of the model and present the scaling/reparameterisation, situating the discussion on innate/adaptive immune responses as used in this paper. In Sec. 3, we present the concept of parasitemia reproduction number as used in this paper, and start the analysis of the mathematical equation by discussing the existence and stability of steady state solutions in Sec. 4. In that section, we prove results on local stability of the parasitized state and on the global stability of the parasite free state. The mathematical analysis is illustrated with some numerical simulations in Sec. 5 and we round up the paper with a discussion and conclusion in Sec. 6.

2. The Within-Human Host Mathematical Model

2.1. *Model equations*

In Ref. 29, we developed a mathematical model that captured the interactions of key population components involved in a malaria positive patient. These populations at any time t, measured in days, are described in Table 1.

The model equations governing the rate of change of the state variables, R_h, R_p, M, G_e, G_l, E_i and E_a, with model schematics shown in Fig. 1, are given in Eqs. (2.1)–(2.7).

$$\frac{dR_h}{dt} = R_h\psi(R_h) - \mu_h R_h - \frac{\beta_1 R_h M}{1+\xi_0 E_a}, \tag{2.1}$$

$$\frac{dR_p}{dt} = \frac{\beta_1 R_h M}{1+\xi_0 E_a} - (\gamma_p + \mu_p)R_p - (\rho_e + \rho_a E_a)R_p E_i, \tag{2.2}$$

Table 1. Description of state variables, measured in cells per unit volume (density) with volume measured in micro-liter (μl).

Variable	Description	Quasi-dimension/Units
$R_h(t)$	Density of healthy red blood cells (HRBCs) at time t.	C = HRBCs $\times\ \mu\text{l}^{-1}$
$R_p(t)$	Density of infected red blood cells (IRBCs) at time t, also known as parasitized red blood cells.	C = IRBCs $\times\ \mu\text{l}^{-1}$
$M(t)$	Density of free floating merozoites at time t. They invade and infect HRBCs.	M = Merozoites $\times\ \mu\text{l}^{-1}$
$G_e(t)$	Density of immature or early state gametocytes at time t. These form are the precursors to the late state gametocytes	G = Gametocytes $\times\ \mu\text{l}^{-1}$
$G_l(t)$	Density of mature or late state gametocytes at time t. These are the transmissible forms of the malaria parasite to mosquitoes, linking the within-human parasite life-cycle to the within-mosquito parasite life cycle. A break in this link would result in an incomplete parasite life-cycle and thus plausible malaria control.	G = Gametocytes $\times\ \mu\text{l}^{-1}$
$E_i(t)$	Density of innate immune system cells at time t. These are the body's natural immune cells that respond to fight invading foreign pathogens. Different cells make up the innate immune system and function in different ways to reduce parasitemia.	I = Immune cells $\times\ \mu\text{l}^{-1}$
$E_a(t)$	Density of adaptive immune system cells at time t. These are malaria parasite specific immune response developed and sustained due to repeated exposure to malaria infection. Different cells make up the adaptive immune response system and these cells function independently to inhibit the parasitemia process or assist the innate immune system in reducing parasitemia.	I = Immune cells $\times\ \mu\text{l}^{-1}$

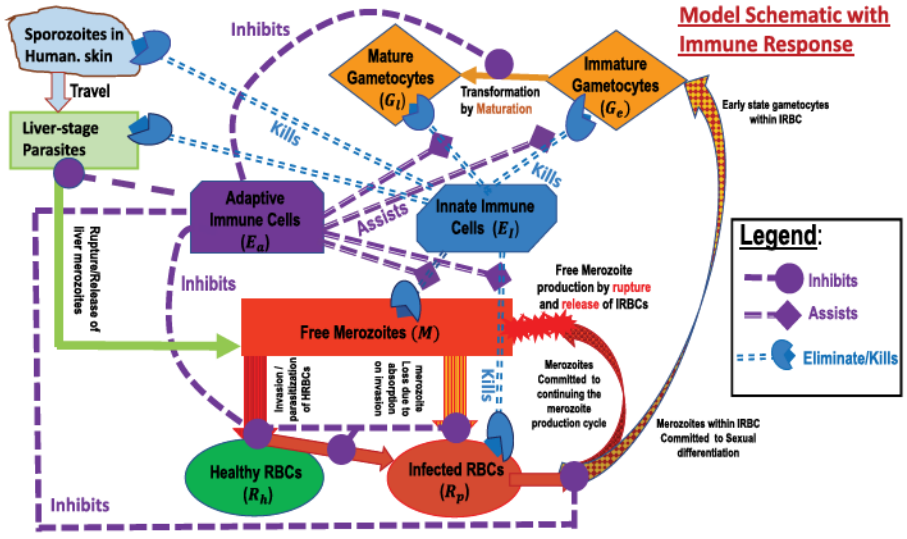

Fig. 1. Model schematics of the within-human host malaria parasite dynamics showing the general complex interaction between the various parasite forms and the innate and adaptive immune systems. Innate immune cells (E_i), can kill (or eliminate) sporozoites from human-skin, free-floating circulating merozoites, IRBCs, immature and mature gametocytes, liver-stage parasites either by direct contact or through phagocytosis. They also help the adaptive immune system in recognizing and capturing antigens using the antigen presenting cells. Adaptive immune cells (E_a), Inhibit/block free floating merozoite invasion of HRBC, maturation of gametocytes, growth of merozoites inside IRBCs, development of liver-stage parasites hence inhibiting the release of liver stage merozoites into blood stream. They also assist and enhance innate immune cells in killing merozoites and also in clearing IRBCs and gametocytes.

$$\frac{dM}{dt} = \frac{r\gamma_p(1-\sigma)R_p}{1+\xi_1 E_a} - \mu_m M - \left(\frac{\beta_2 R_h}{1+\xi_0 E_a} + \frac{\beta_3 R_p}{1+\xi_0 E_a} + (\rho_m + \rho_n E_a)E_i\right) M, \tag{2.3}$$

$$\frac{dG_e}{dt} = \frac{s\sigma\gamma_p R_p}{1+\xi_1 E_a} - (\gamma_l + \mu_e)\, G_e - (\rho_g + \rho_q E_a)E_i G_e, \tag{2.4}$$

$$\frac{dG_l}{dt} = \frac{\gamma_l G_e}{1+\xi_2 E_a} - \mu_l G_l - \rho_l E_i G_l, \tag{2.5}$$

$$\frac{dE_i}{dt} = H_i(E_i) + \Gamma_1(R_p, M, E_i), \tag{2.6}$$

$$\frac{dE_a}{dt} = \Gamma_2(R_p, M, E_a) - \mu_a E_a, \tag{2.7}$$

together with the following specified initial conditions defined at some initial time, $t = t_0$,

$$\begin{aligned} &R_h(t_0) = R_{0h}, \quad R_p(t_0) = 0, \quad M(t_0) = M_0, \quad G_e(t_0) = 0, \\ &G_l(t_0) = 0, \quad E_i(t_0) = E_{0i}, \quad E_a(t_0) = 0. \end{aligned} \tag{2.8}$$

In Eq. (2.8), $R_{0h}, M_0 > 0$ and $E_{0i} \geq 0$. Changes to the immune variables, E_i and E_a, as shown in Eqs. (2.6)–(2.7), are modeled in terms of general functions $\Gamma_1(R_p, M, E_i)$ and $\Gamma_2(R_p, M, E_a)$, designed to capture the interaction between merozoites, IRBCs, and the innate and adaptive immune cells.

Equations (2.1)–(2.5) and (2.6)–(2.7) for the specific example were $\Gamma_1(R_p, M, E_i) = \vartheta_1 R_p + \vartheta_2 M - (\lambda_1 R_p + \lambda_2 M)E_i$ and $\Gamma_2(R_p, M, E_a) = \varrho_1 R_p + \varrho_2 M - (\theta_1 R_p + \theta_2 M)E_a$, derived based on some simplifying assumptions, were developed and described detail in Refs. 29 and 42. Since, we have made some updates, and for ease of understanding the model system (2.1)–(2.7), we give a summary below. The associated parameters to system (2.1)–(2.7) are described in Table 2.

The density of HRBCs, R_h, changes due to a net increase from the production of mature HRBCs from precursor cells from the bone marrow, modeled via the function $R_h\psi(R_h)$, elaborated upon in Sec. 2.2. The recruitment depends on the current state of HRBCs in the human system. Decrease in density of HRBC is either due to natural death at the per capita rate μ_h, or due to parasitization by merozoites, modeled via $\frac{\beta_1 R_h M}{1+\xi_0 E_a}$, a process inhibited by adaptive immune cells, where $\xi_0 \geq 0$ quantifies the inhibitive efficiency of the adaptive immune cells' action on the parasitization process. Parasitization of HRBCs by free-floating merozoites increases the parasitized red blood cell (IRBC) population, R_p. This population is decreased due to either natural death at the per capita rate μ_p or as a result of a change in the parasite course at rate γ_p per infected red blood cell. The time $1/\gamma_p$ is the time IRBCs either rupture to release free-floating merozoites or continue the path to gametocytogenesis. IRBC density is also decreased as a result of action via contact with innate immune cells ($\rho_e R_p E_i$) or as a result of the combined interaction with innate and adaptive immune cells ($\rho_a E_a R_p E_i$).

Various cells make up the innate and adaptive immune cells, and their action on parasite forms or IRBCs are different. In summary, innate immune cells kill sporozoites on human skin, eliminate circulating free-floating merozoites as well as IRBCs and early and late state gametocytes. They also limit the development of liver-stage parasites thereby suppressing the infection development at this stage. They function either through direct contact with parasite forms and IRBCs or through phagocytosis whereby parasites are killed by recognition through the innate immune receptors and/or in conjunction with adaptive immune cells. Innate immune cells also help adaptive immune cells capture and process antigens using antigen presenting cells. In addition to their combined action with innate immune cells in merozoite killing and enhanced clearance of IRBCs, adaptive immune cells also inhibit or block merozoite invasion of HRBCs, bursting of red blood cells, as well as the maturation of gametocytes, the development of parasites in an IRBC and the development and release of liver-stage parasite. Thus, it is a complex process and the details have been tabulated in Supplemental document A.

A fraction, $(1 - \sigma)$, of IRBCs will rupture releasing up to r free-floating merozoites per bursting red blood cells and the process increases the density

Table 2. Description of model parameters and their quasi-dimension as given in Ref. 29.

Parameter	Description	Quasi-dimension
β_1	Mass action contact rate between free floating merozoites and HRBCs, modeling the effective parasitization rate of HRBCs by merozoites.	$M^{-1}T^{-1}$
β_2	Adjusted mass action contact rate between free floating merozoites and HRBCs, modeling effective absorption rate of free merozoites by red blood cells as the merozoites attempt to invade the cells. The merozoites are cleared from the blood stream in the process.	$C^{-1}T^{-1}$
β_3	Mass action contact rate between free floating merozoites and IRBCs, modeling the effective absorption rate of free merozoites by IRBCs as the merozoites attempt to invade the cells. The merozoites are cleared from the blood stream in the process.	$C^{-1}T^{-1}$
Θ	Constant recruitment rate of HRBCs.	CT^{-1}
μ_h	Per capita natural death rate of HRBCs.	T^{-1}
$\tilde{\mu}_h$	Additional HRBCs density-dependent death rate due to self-limiting processes for large densities.	$C^{-1}T^{-1}$
λ_h	Growth rate of HRBCs due to per capita production of HRBCs.	T^{-1}
μ_p	Per capita natural linear death rate of IRBCs.	T^{-1}
μ_e	Per capita natural linear death rate of immature gametocytes.	T^{-1}
μ_l	Per capita natural linear death rate of mature gametocytes.	T^{-1}
μ_m	Per capita natural linear death rate of freely floating merozoites.	T^{-1}
μ_i	Per capita natural death rate of innate immune cells.	T^{-1}
μ_a	Per capita natural linear death rate of adaptive immune cells.	T^{-1}
δ_i	Linear growth rate of innate immune system cells.	T^{-1}
K_i	Carrying capacity of the environment for innate immune system cells.	I
M_i	Threshold innate immune system cell size below which the innate immune system cells become ineffective. We expect $0 < M_i < K_i$.	I
ξ_0	Efficiency of the adaptive immune effectors in inhibiting merozoite contact with HRBCs and IRBCs via mass action contact.	I^{-1}
ξ_1	Efficiency of the adaptive immune effectors in inhibiting merozoite transformation in parasitized or infected red blood cells.	I^{-1}
ξ_2	Efficiency of the adaptive immune effectors in inhibiting maturation of early state gametocytes.	I^{-1}
ρ_e	Mass action contact rate between parasitized red blood cells and innate immune system cells resulting in the elimination of the parasitized cells.	$I^{-1}T^{-1}$
ρ_m	Mass action contact rate between free floating merozoites and innate immune system cells. This contact can result in the elimination of the free floating merozoites.	$I^{-1}T^{-1}$
ρ_g	Mass action contact rate between immature gametocytes and innate immune system cells. This contact can result in the elimination of the immature gametocytes.	$I^{-1}T^{-1}$
ρ_l	Mass action contact rate between mature gametocytes and innate immune system cells resulting in mature gametocyte elimination.	$I^{-1}T^{-1}$

Table 2. (*Continued*)

Parameter	Description	Quasi-dimension
ρ_a	Mass action contact rate between IRBCs, innate immune system cells and adaptive immune system cells accounting for additional clearances due to the presence of adaptive immunity.	$I^{-2}T^{-1}$
ρ_n	Mass action contact rate between merozoites, innate immune system cells and adaptive immune system cells, accounting for additional clearances due to the presence of adaptive immunity.	$I^{-2}T^{-1}$
ρ_q	Mass action contact rate between immature gametocytes, innate immune system cells and adaptive immune system cells, accounting for additional clearances due to presence of adaptive immunity.	$I^{-2}T^{-1}$
r	Average number of merozoites released per bursting IRBC.	MC^{-1}
s	Average number of early stage gametocytes arising from one IRBC.	GC^{-1}
σ	A parameter in $[0,1]$, it is the proportion of the IRBCs that differentiate continuing towards the path to gametocytogenesis.	1
γ_p	rate of maturation per IRBC to a point where the IRBC either bursts to release more free merozoites or continue towards the gametocyte formation path called gametocytogenesis.	T^{-1}
γ_l	Transition rate of immature gametocytes mature within an IRBC.	T^{-1}
ϑ_1	Rate at which innate immune effectors are stimulated/generated due to the presence of IRBCs.	$IC^{-1}T^{-1}$
ϑ_2	Rate at which innate immune effectors are stimulated/generated due to the presence of free-floating merozoites.	$IM^{-1}T^{-1}$
ϱ_1	Rate which adaptive immune effectors are stimulated/generated due to the presence of IRBCs.	$IC^{-1}T^{-1}$
ϱ_2	Rate which adaptive immune effectors are stimulated/generated due to the presence of free floating merozoites.	$IM^{-1}T^{-1}$
λ_1	Mass action contact rate between IRBCs and innate immune system cells accounting for the loss of innate immune cells due to such contact.	$C^{-1}T^{-1}$
λ_2	Mass action contact rate between free merozoites and innate immune system cells accounting for the loss of innate immune cells due to such contact.	$M^{-1}T^{-1}$
θ_1	Mass action contact rate between IRBCs and adaptive immune system cells accounting for the loss of the adaptive immune cells due to such contact.	$C^{-1}T^{-1}$
θ_2	Mass action contact rate between free-merozoites and adaptive immune system cells accounting for adaptive immune cell loss due to such contact.	$M^{-1}T^{-1}$

of free-floating merozoites. The remaining fraction, σ, that does not burst continue the path to gametocytogenesis, increasing in the early state gametocyte density. Both processes, Inhibited by the adaptive immune cells, are modeled via the terms $\frac{r\gamma_p(1-\sigma)R_p}{1+\xi_1 E_a}$ and $\frac{s\gamma_p\sigma R_p}{1+\xi_1 E_a}$, where $\xi_1 \geq 0$ quantifies the inhibitive efficiency of the adaptive immune cells' action on IRBCs bursting or continuation to gametocytogenesis. The densities of both merozoites and early state gametocytes

are reduced due to natural death at the per capita rates of μ_m and μ_e, respectively, or as a result of contact with innate immune cells (modeled via $\rho_m M E_i$ and $\rho_g G_e E_i$, respectively) or as a result of the combined interaction with innate and adaptive immune cells (modeled via $\rho_n E_a M E_i$ and $\rho_q E_a G_e E_i$, respectively). Additional losses occur in the merozoite population as a result of the merozoites infecting or parasitizing red blood cells, resulting in them being absorbed (see Refs. 43 and 44 for details). We model these by the terms $\frac{\beta_2 R_h M}{1+\xi_0 E_a}$ and $\frac{\beta_3 R_p M}{1+\xi_0 E_a}$, where $\xi_0 \geq 0$ measures the efficiency of the adaptive immune cells' action on inhibiting the parasitization process. Early state gametocytes that successfully evade the inhibitive properties of the adaptive immune cells serve as the precursors to the mature gametocyte population, producing $\frac{\gamma_l G_e}{1+\xi_2 E_a}$ late state gametocytes. Here, γ_l is the maturation rate and $\xi_2 \geq 0$ quantifies the maturation inhibitive efficiency. The population of mature gametocytes diminishes due to natural death at rate μ_l or as a result of innate immune action in fighting this foreign body, modeled by $\rho_l E_i G_i$.

In model (2.1)–(2.7), the functions $\psi, H_i : \mathbb{R}^+ \to \mathbb{R}$ are needed to model the rate of recruitment of new red blood cells and innate immune effector cells, respectively. We motivate the nature and properties that a realistic recruitment function should have in our context. The choices of the recruitment functions in (2.1)–(2.7) serve as a generalizes of past works on the within-human malaria parasite dynamics (see for example, Refs. 25, 28, 41, 43, 45 and 46).

2.2. *The recruitment functions*

In the absence of malaria infection in a human, the equation governing the HRBC density is

$$\frac{dR_h}{dt} = R_h \psi(R_h) - \mu_h R_h \equiv \tilde{g}(R_h), \tag{2.9}$$

where it is assumed that erythrocytes are recruited from the stems of the bone marrow at a density-dependent rate $\psi(R_h)$ per healthy red blood cell and have a life expectancy of $1/\mu_h$. The term $\mu_h R_h(t)$ therefore represents the net rate of erythrocytes dying naturally in a healthy human body. Our objective in this subsection is to discuss conditions on the form of $\psi : [0, \infty) \to \mathbb{R}$ that can serve as a suitable red blood cell recruitment function for our model. We have deliberately assumed for simplicity as in Refs. 47 and 48, that the recruitment function (even in the presence of infection) depends only on the density of healthy erythrocytes R_h but not on the total density of healthy and infected erythrocytes, even though it has been conjectured that the production of erythrocytes is accelerated in a small way by the presence of infected erythrocytes in the system.[25] We assume that the function $\psi : [0, \infty) \to \mathbb{R}$ has required properties that will guarantee the existence of a healthy erythrocyte population so that the growth dynamics of healthy erythrocytes in the absence of malaria parasites is internally stable, from a mathematical and physical stand point. We write down the following definition for HRBC recruitment functions.

Definition 1 (Recruitment functions). For the sake of mathematical and biological realism, a function $\psi : [0, \infty) \to \mathbb{R}$ is considered to be a suitable recruitment rate function if it is smooth and in addition should satisfy the following conditions:

(1) $\psi(0_+) > 0$, $\psi(R_h) \geq 0$, $\forall R_h \geq 0$, where $\psi(0_+) = \lim_{R_h \to 0^+} \psi(R_h)$.
(2) $\psi'(R_h)$ exists for all $R_h \geq 0$ and $\psi'(R_h) < 0$, $\forall R_h \geq 0$.
(3) $\lim_{R_h \to +\infty} \psi(R_h) \leq \mu_h < \lim_{R_h \to 0^+} \psi(R_h)$, $\forall R_h > 0$.
(4) The function $R_h\psi(R_h)$ is non-negative, continuously differentiable, bounded and unimodal so that there exists $R_h^m > 0$ such that for $0 < R_h < R_h^m$, $R_h\psi(R_h)$ is strictly monotone increasing and for $R_h > R_h^m$, $R_h\psi(R_h)$ is strictly monotone decreasing.

Condition (1) ensures non-negativity of ψ and $R_h\psi(R_h)$, with $R_h\psi(R_h)$ representing the net rate of production of new R_h per time. Condition (2) ensures that ψ is a monotone decreasing function of its argument, meanwhile condition (3) ensures that Eq. (2.9), which models the dynamics of HRBCs in the absence of infection, has a nonzero stationary solution R_h^* such that $R_h^* = \psi^{-1}(\mu_h)$, which is stable to small perturbations. Additionally, it ensures that a carrying capacity, denoted by C, exists such that for $R_h < C$, R_h is increasing with time (since $R_h' > 0$), and for $R_h > C$, $R_h' < 0$ implying that R_h is decreasing with time t. Condition (4) ensures that $R_h\psi(R_h)$ has a positive maximum value given by $\hat{R}_h\psi(\hat{R}_h)$, where $\hat{R}_h \in [0, \infty)$ satisfies the equation $\psi(\hat{R}_h) + \hat{R}_h\psi'(\hat{R}_h) = 0$, and allowable shapes for the graph of $R_h\psi(R_h)$ are shown in Fig. 2. Examples of recruitment functions in population dynamics that satisfy (1)–(4) may be found in Refs. 13 and 49. Some of these are mentioned below in the context this work:

(a) **The linear recruitment function:** Here, we consider $\psi(R_h) = \frac{\Theta}{R_h}$, where $\Theta > 0$ is a constant, so that in the absence of infection, the HRBCs equation, namely, $R_h'(t) = \tilde{g}(R_h(t)) = \Theta - \mu_h R_h(t)$ is the constant recruitment linear death growth model in biology.
(b) **The logistic recruitment function:** For this case, we consider the function $\psi(R_h) = \lambda_h - \tilde{\mu}_h R_h$, where $\lambda_h > \mu_h$ is the per capita constant rate of recruitment of HRBCs from bone marrow and $\tilde{\mu}_h$ is additional death rate per HRBCs. The assumption is that a self limiting process kicks in for large densities, inducing additional HRBC deaths. In this case, the HRBC dynamics in the absence of infection is modeled by $R_h'(t) = \tilde{g}(R_h) = (\lambda_h - \mu_h)R_h(1 - \frac{\tilde{\mu}_h}{(\lambda_h - \mu_h)}R_h)$, which is effectively the logistic growth model in biology,[a] originally proposed

[a]The action of HRBC production from the precursors (see Ref. 50) is masked in the present formulation. The chosen form should be understood as follows: In the absence of malaria disease and under steady state, $\lambda_h = \mu_h$ and $\tilde{\mu}_h = 0$. If there is a decline in the HRBC density, then $\lambda_h > \mu_h$, where the processes and feedback loops leading to the increased production of HRBCs from the precursors have not been explicitly modeled. Likewise, if the HRBC density is too large, then $\lambda_h < \mu_h$, in addition to $\tilde{\mu}_h > 0$, with its size dependent on the density of HRBCs.

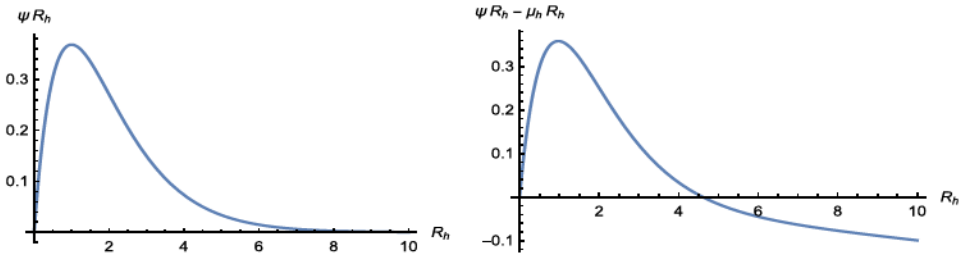

(a) (b)

Fig. 2. Figure showing the allowable shape and behavior of the dynamics for any choice of ψ leading to the net recruitment function $R_h\psi(R_h)$ in the equation for the time rate of change of HRBCs in the absence of infection (2.9). The function $\psi : [0, \infty) \to \mathbb{R}$ is to be chosen so that the $R_h\psi(R_h)$ is a unimodal function graph (a), and the dynamic described by the function $\tilde{g}(R_h) = R_h\psi(R_h) - \mu_h R_h$ crosses the R_h axis at exactly one point as shown in (b) implying the existence of a unique stable steady state solution for the equation $R_h'(t) = \tilde{g}(R_h(t)), R_h(0) = R_h^0 \in (0, \infty)$.

by Verhulst[51] and used by Pearl.[52] It is worth noting, however, that this form of ψ does not satisfy the positivity condition prescribed by condition (1) of Definition 1 when $R_h > \frac{\lambda_h}{\mu_h}$, but we assume that, in this case, $\frac{\lambda_h}{\mu_h}$ is sufficiently large.

(c) **The Ricker recruitment function:** In the third instance, we consider $\psi(R_h) = \lambda_h e^{-\frac{1}{K_h}R_h}$ where λ_h and K_h are positive constants. K_h may be associated with the environmental carrying capacity, while λ_h can be seen as the limiting HRBC production rate when the HRBC count is very low. We demand that $\lambda_h > \mu_h$ so that in the absence of infection, the dynamic of the HRBC population is modeled by the Ricker growth model[53] where $R_h'(t) = \tilde{g}(R_h) = R_h(\lambda_h e^{-\frac{1}{K_h}R_h} - \mu_h)$. The Ricker growth function has also been used by Nisbet and Gurney[54] to model laboratory fly populations.

(d) **The Maynard–Smith–Slatkin recruitment function:** In the fourth instance, we consider $\psi(R_h) = \lambda_h\left(1 + \left(\frac{R_h}{K_h}\right)^n\right)^{-1}$ where this form of the recruitment function for $n \neq 1$ is known as the Maynard–Smith–Slatkin birth rate function,[55] and for $n = 1$ is the Beverton–Holt recruitment function.[56] With this type of recruitment function, n is a measure of the degree of nonlinearity in the recruitment function so that larger values of n provide stronger nonlinear response functions. We note that to stay within the limitations set by the requirements on the recruitment function as specified by Definition 1 and illustrated in Fig. 2, we must impose the restriction $n > 1$. In the absence of the disease, $R_h'(t) = \tilde{g}(R_h) = \lambda_h R_h\left(1 + \left(\frac{R_h}{K_h}\right)^n\right)^{-1} - \mu_h R_h$. λ_h has the same interpretation as in the Ricker case and we again assume that $\lambda_h > \mu_h$ so that when cell numbers are small, deaths do not predominate births. The Maynard–Smith–Slatkin growth rate function has also been used by Ngonghala *et al.*[13] and Ngwa *et al.*[18] in modeling mosquito population dynamics.

We clarify the notion of linearity and nonlinearity as used in the study presented in this paper with the following definition.

Definition 2 (Linear versus nonlinear recruitment functions). In light of the different functions $\psi : [0, \infty) \to \mathbb{R}$ defined above and satisfying Definition 1, we refer to the function $\tilde{g} : [0, \infty) \to \mathbb{R}$ defined by $\tilde{g}(R_h) = R_h\psi(R_h) - \mu_h R_h$ as (i) a linear recruitment function if $\tilde{g}(R_h)$ is at most a polynomial of degree one in R_h, and (ii) a nonlinear recruitment function if $\tilde{g}(R_h)$ is either a polynomial of degree at least two in R_h or a combination of rational/irrational and transcendental functions of R_h. Furthermore, we shall refer to $\tilde{g}(R_h)$ as a more (or strongly) nonlinear recruitment function if any attempt to write $\tilde{g}(R_h)$ as a complete and convergent power series will always result in an infinite power series representation in powers of R_h.

In the context of Definition 2, combinations of exponential and polynomial functions that admit infinite power series expansions with the desired properties delimited by Definition 1 are admissible recruitment functions.

Similar functional forms can be selected and used for the recruitment of innate immune effector cells (see (2.6)) modeled via the function $H_i : [0, \infty) \to \mathbb{R}$. Three example cases are: (i) linear model: $H_i = \Theta_i - \mu_i E_i$, with Θ_i constant recruitment and μ_i the per capita death rate; (ii) Verhulst–Pearl logistic model, $H_i(E_i) = \delta_i E_i\big(1 - \frac{E_i}{K_i}\big)$, where δ_i is the net linear per capita growth rate of innate immune system cells and $K_i > 0$ is the carrying capacity of the environment for innate immune system cells and (iii) model with allee effect: $H_i(E_i) = \delta_i E_i\big(1 - \frac{E_i}{K_i}\big)\big(\frac{E_i}{M_i} - 1\big)$, with δ_i and K_i as given in (ii). This example accounts for allee effects, with M_i the allee threshold density marking the immune system cell density switch point below which the innate immune density is no longer effective. For a meaningful and effective switch, $0 < M_i < K_i$. A systematic consideration of the different possible combinations of the different types of recruitment functions for the HRBCs and innate immune effector cells represented in this paper will result in consideration of several different models for the within human host dynamics of the malaria parasite in the presence of immunity. The fact that different forms of recruitment functions that fall within the expected realities in modeling can be formulated, leads us to the possibility of considering a large class of models of the type studied herein.

In the presence of malaria infection, a human's innate as well as adaptive, for mature-immune humans, immune systems are boosted by the presence of the infection. This boosts results in interactions between the immune cells, IRBCs and some parasite forms. In particular, during infection and in the presence of immunity, IRBCs (R_p), free-floating merozoites (M) and the early state gametocytes (G_e), interact and are affected by both the innate and adaptive immune systems while the late state gametocytes, (G_l), is affected by the innate immune system. The interaction also yields losses to the immune cell densities (since elimination is assumed to be done by phagocytosis when the immune cells come in contact with the free-floating merozoites and IRBCs). In Eqs. (2.6) and (2.7), we model the interactions by general functions $\Gamma_1(R_p, M, E_i)$ and $\Gamma_2(R_p, M, E_a)$ which

would be chosen to capture such a loss and such that in the absence of infection whereby $R_p = M = 0, \forall t > 0$, $\Gamma_1 = \Gamma_2 = 0$. That is, based on Eq. (2.7), the adaptive immune system cells will wane at the constant per capita rate of μ_a. This makes sense biologically, since the dynamics of the adaptive immune response is maintained by continued presence of infection in the human body. Thus, from (2.7), in the absence of the malaria infection, E_a will decay exponential decay to zero according to the relation $E_a \propto \exp(-\mu_a t)$. As earlier noted, the simple forms in which $\Gamma_1(R_p, M, E_i) = \vartheta_1 R_p + \vartheta_2 M - (\lambda_1 R_p + \lambda_2 M)E_i$ and $\Gamma_2(R_p, M, E_a) = \varrho_1 R_p + \varrho_2 M - (\theta_1 R_p + \theta_2 M)E_a$, were used in Refs. 29 and 42, to model the interactions between innate and adaptive immune cells and IRBCs and parasite forms, with the added assumption that $\varrho_1 \leq \varrho_2$, $\theta_1 \leq \theta_2$, $\vartheta_1 \leq \vartheta_2$ and $\lambda_1 \leq \lambda_2$, so as to account for the reduced elimination of IRBCs by immune cells E_i and E_a, compared to their effect on free-floating merozoites.[46] For the adaptive immune example, the form of $\Gamma_2(R_p, M, E_a)$ neglects the delay associated with the time adaptive immune system takes to develop within an individual.

Here, we will not explicitly model the dynamics of both the adaptive and innate immune system cells, but consider their effects on the model system (2.1)–(2.7) at fixed time points where by the model steady states and parasitemia threshold, denoted by $\mathscr{R}_0$, are obtained as functions of immune variables and analyzed at snapshots of immune sizes. In the absence of information for the true form of the recruitment function, we maintain that the results of this analysis will give an insight into the nature of the within human host dynamics of the malaria parasite. In what follows, even though we have written down two equations, what we now refer to as prototype equations for the immune response, we shall regard the presence of the activity of immune response in the system as parametric variables and derive all formulae in terms of these parametric variables.

The basic properties of invariance, positivity, boundedness and uniqueness of solutions to system (2.1)–(2.7) with initial conditions in (2.8) and under the conditions given for $\psi(R_h)$ and $H_i(E_i)$ as stated in this section, were established in Refs. 22 and 29, when the HRBCs, in the absence of parasitemia, are modeled by the linear and logistic models. The results are easily extendable to the Ricker and Maynard–Smith–Slatkin recruitment functions and are not presented here.

2.3. *Reparameterisation, scaling and nondimensionalization*

Following the idea in Ref. 29, expanded to incorporate all four recruitment functions discussed in Sec. 2.2, we nondimensionalize as follows: We begin by letting

$$\begin{aligned} r_h &= \frac{R_h}{R_h^0}, \quad r_p = \frac{R_p}{R_p^0}, \quad \tau = (\mu_p + \gamma_p)t, \quad m = \frac{\beta_2 M}{r\gamma_p}, \quad g_e = \frac{(\mu_e + \gamma_l)G_e}{s\gamma_p R_p^0}, \\ g_l &= \frac{\mu_l(\mu_e + \gamma_l)G_l}{\gamma_l(s\gamma_p R_p^0)}, \quad e_i = \frac{E_i}{E_i^0}, \quad e_a = \frac{(\mu_p + \gamma_p)E_a}{\varrho_1 R_p^0}, \end{aligned} \tag{2.10}$$

where R_0^0, R_p^0 and E_i^0 are given as

$$R_h^0 = R_p^0 = \begin{cases} \dfrac{\Theta}{\mu_h} & \text{if } \psi(R_h) = \dfrac{\Theta}{R_h}, \\ \dfrac{\lambda_h - \mu_h}{\tilde{\mu}_h} & \text{if } \psi(R_h) = \lambda_h - \tilde{\mu}_h R_h, \\ -K_h \ln(\mu) & \text{if } \psi(R_h) = \lambda_h e^{-\frac{1}{K_h} R_h}, \\ K_h \left(\dfrac{1}{\mu} - 1\right)^{\frac{1}{n}} & \text{if } \psi(R_h) = \lambda_h \left(1 + \left(\dfrac{R_h}{K_h}\right)^n\right)^{-1}, \end{cases} \tag{2.11}$$

$$E_i^0 = \begin{cases} \dfrac{\Theta_i}{\mu_i} & \text{if } H(E_i) = \Theta_i - \mu_i E_i, \\ K_i & \text{if } H(E_i) = \delta_i E_i \left(1 - \dfrac{E_i}{K_i}\right) \text{ or} \\ & H(E_i) = \delta_i E_i \left(1 - \dfrac{E_i}{K_i}\right)\left(\dfrac{E_i}{M_i} - 1\right), \end{cases}$$

and the dimensionless parameter groupings are

$$K = \frac{M_i}{K_i}, \quad \mu = \frac{\mu_h}{\lambda_h},$$

$$a_0 = \begin{cases} \dfrac{\mu_h}{\mu_p + \gamma_p} & \text{if } \psi(R_h) = \dfrac{\Theta}{R_h}, \\ \dfrac{\lambda_h - \mu_h}{\mu_p + \gamma_p} & \text{if } \psi(R_h) = \lambda_h - \tilde{\mu}_h R_h, \\ \dfrac{\lambda_h}{\mu_p + \gamma_p} & \text{if } \psi(R_h) = \lambda_h e^{-\frac{1}{K_h} R_h} \text{ or } \psi(R_h) = \lambda_h \left(1 + \left(\frac{R_h}{K_h}\right)^n\right)^{-1}, \end{cases}$$

$$a_1 = \frac{r\gamma_p \beta_1}{\beta_2(\mu_p + \gamma_p)}, \quad a_2 = \frac{\beta_2 R_h^0}{\mu_p + \gamma_p}, \quad a_3 = \frac{\mu_m}{\mu_p + \gamma_p},$$

$$a_4 = \frac{\mu_e + \gamma_l}{\mu_p + \gamma_p}, \quad a_5 = \frac{\mu_l}{\mu_p + \gamma_p}, \quad a_6 = \frac{\mu_a}{\mu_p + \gamma_p},$$

$$\rho_1 = \frac{\rho_e E_i^0}{\mu_p + \gamma_p}, \quad \rho_2 = \frac{\rho_a \varrho_1 R_p^0}{\rho_e(\mu_p + \gamma_p)}, \quad \rho_3 = \frac{\rho_m E_i^0}{\mu_p + \gamma_p},$$

$$\rho_4 = \frac{\rho_n \varrho_1 R_p^0}{\rho_m(\mu_p + \gamma_p)}, \quad \rho_5 = \frac{\rho_g E_i^0}{\mu_p + \gamma_p}, \quad \rho_6 = \frac{\rho_q \varrho_1 R_p^0}{\rho_g(\mu_p + \gamma_p)},$$

$$\rho_7 = \frac{\rho_l E_i^0}{\mu_p + \gamma_p}, \quad p_0 = \frac{\xi_0 \varrho_1 R_p^0}{\mu_p + \gamma_p}, \quad p_1 = \frac{\xi_1 \varrho_1 R_p^0}{\mu_p + \gamma_p}, \quad p_2 = \frac{\xi_2 \varrho_1 R_p^0}{\mu_p + \gamma_p}, \quad \beta = \frac{\beta_3}{\beta_2},$$

$$b_1 = \frac{\vartheta_1 R_p^0}{E_i^0(\mu_p+\gamma_p)}, \quad b_2 = \frac{\vartheta_2 r\gamma_p}{\vartheta_1\beta_2 R_p^0}, \quad b_3 = \frac{\varrho_2 r\gamma_p}{\varrho_1\beta_2 R_p^0},$$
$$c_1 = \frac{\lambda_1 R_p^0}{\mu_p+\gamma_p}, \quad c_2 = \frac{\lambda_2 r\gamma_p}{\lambda_1\beta_2 R_p^0}, \quad c_3 = \frac{\theta_1 R_p^0}{\mu_p+\gamma_p},$$
$$c_4 = \frac{\theta_2 r\gamma_p}{\theta_1\beta_2 R_p^0},$$
$$\delta = \begin{cases} \dfrac{\mu_i}{\mu_p+\gamma_p} & \text{if } H(E_i) = \Theta_i - \mu_i E_i, \\ \dfrac{\delta_i}{\mu_p+\gamma_p} & \text{if } H(E_i) = \delta_i E_i\left(1-\dfrac{E_i}{K_i}\right) \text{ or} \\ & \quad H(E_i) = \delta_i E_i\left(1-\dfrac{E_i}{K_i}\right)\left(\dfrac{E_i}{M_i}-1\right). \end{cases} \tag{2.12}$$

We note that μ as defined in Eq. (2.12) satisfies $0 < \mu \leq 1$. Substituting Eqs. (2.10)–(2.12) into Eqs. (2.1)–(2.7), we obtain the scaled system

$$\frac{dr_h}{d\tau} = a_0 g(r_h) - \frac{a_1 m r_h}{1+p_0 e_a}, \tag{2.13}$$
$$\frac{dr_p}{d\tau} = \frac{a_1 m r_h}{1+p_0 e_a} - r_p - \rho_1(1+\rho_2 e_a) r_p e_i, \tag{2.14}$$
$$\frac{dm}{d\tau} = a_2\left[\frac{(1-\sigma)r_p}{1+p_1 e_a} - m\left(\frac{r_h}{1+p_0 e_a} + \frac{\beta r_p}{1+p_0 e_a}\right)\right] - a_3 m - \rho_3(1+\rho_4 e_a) e_i m, \tag{2.15}$$
$$\frac{dg_e}{d\tau} = a_4\left[\frac{\sigma r_p}{1+p_1 e_a} - g_e\right] - \rho_5(1+\rho_6 e_a) e_i g_e, \tag{2.16}$$
$$\frac{dg_l}{d\tau} = a_5\left[\frac{g_e}{1+p_2 e_a} - g_l\right] - \rho_7 e_i g_l, \tag{2.17}$$
$$\frac{de_i}{d\tau} = h(e_i) + \widetilde{\Gamma}_1(e_i, r_p, m), \tag{2.18}$$
$$\frac{de_a}{d\tau} = \widetilde{\Gamma}_2(e_i, r_p, m) - a_6 e_a, \tag{2.19}$$

together with the equations

$$g(r_h) = \begin{cases} 1-r_h & \text{if } \psi(R_h) = \dfrac{\Theta}{R_h}, \\ r_h(1-r_h) & \text{if } \psi(R_h) = \lambda_h - \tilde{\mu}_h R_h, \\ r_h e^{r_h \ln(\mu)} - \mu r_h & \text{if } \psi(R_h) = \lambda_h R_h e^{-\frac{1}{K_h}R_h}, \\ \dfrac{r_h}{1+(\frac{1}{\mu}-1)r_h^n} - \mu r_h & \text{if } \psi(R_h) = \lambda_h\left(1+\left(\frac{R_h}{K_h}\right)^n\right)^{-1}, \end{cases} \tag{2.20}$$

$$h(e_i) = \begin{cases} \delta(1-e_i) & \text{if } H(e_i) = \Theta_i - \mu_i E_i, \\ \delta e_i(1-e_i) & \text{if } H_i(E_i) = \delta_i E_i \left(1 - \dfrac{E_i}{K_i}\right), \\ \delta e_i(1-e_i)\left(\dfrac{e_i}{K} - 1\right) & \text{if } H_i(E_i) = \delta_i E_i \left(1 - \dfrac{E_i}{K_i}\right)\left(\dfrac{E_i}{M_i} - 1\right). \end{cases} \tag{2.21}$$

As noted in Table 2, $0 < M_i < K_i \Rightarrow 0 < K < 1$. Thus, in the third case of Eq. (2.21), K represents the innate immunity threshold below which the innate immune response becomes less effective. Using the prototype examples earlier discussed and modeled in Refs. 29 and 42, the nondimensional forms of $\widetilde{\Gamma}_1$ and $\widetilde{\Gamma}_2$ are $\widetilde{\Gamma}_1(e_i, r_p, m) = b_1(r_p + b_2 m) - c_1(r_p + c_2 m)e_i$ and $\widetilde{\Gamma}_2(e_i, r_p, m) = r_p + b_3 m - c_3(r_p + c_4 m)e_a$. A complete discussion including relative sizes of the scaled parameters of system (2.13)–(2.17), together with a subcase of (2.20) and (2.21), under immune suppression, was presented in Ref. 29. In particular, $0 \leq \sigma \leq 1$, $0 < \beta \leq 1$, $a_0 \in (0,1)$ for the linear case where $g(r_h) = 1 - r_h$ and $a_0 > 0$ for all other forms of $g(r_h)$, $a_1 \geq 0$, $a_2 > 0$, $a_3 > 1$ and $0 < a_4, a_5 < a_3$.

2.4. *The innate and adaptive immune responses*

In a generalized setting, we will analyze system (2.13)–(2.19) and in the process attempt to quantify the level of immune presence in the system, which we know is quite variable in different individuals. Here, we do not pursue this approach. Rather, we work with the general assumption that the net effect of the action of the immune system is to slow down, if not arrest, the process of invasion by the pathogen of the human biological system. This "slowing down effect" has been captured in the model above through the inclusion of the terms of the form $\frac{1}{1+p_k e_a}$ and $-\rho_i(1 + \rho_{i+1} e_a)e_i$, $k = 0, 1, 2$ and $i = 1, \ldots, 7$ in the model equations (2.13)–(2.17) where e_i is the dimensionless density of innate immune effector cells while e_a is that of adaptive immune effector cells. It is understood that the innate immunity is the front-line active immune effector cells that are produced and are always present in the system at all times. In the context of the scaling done above, we assume that e_i is scaled with its maximum possible size so that $0 \leq e_i \leq 1$. $e_i = 0$ is the lack of natural immune effector cells characteristic of two scenarios: one where the immune system has been totally compromized by infection, malaria parasite or other, and the other arising where the individual has never been exposed to malaria infection but other factors compromises the system. On the other hand adaptive immunity kicks in and is sustained by continuing exposure to malaria, but also wanes away when the exposure is stopped over a long period of time. That is, the effectiveness of the adaptive immune response increases with duration of infectivity and frequency of exposure to the infection. However, since this increase cannot be indefinite, we assume that e_a, with $e_a \geq 0$, is also bounded, with a bound

determined by the size and frequency of exposure to malaria infection as well as the length of sustained infectivity state. The case $e_a = 0$ commensurate with the scenario where an individual has had no exposure to malaria over a long period of time. Without diving into the specifics of actually computing the size of the immune states of the individual in a full and complete mathematical analysis of the coupled system (2.13)–(2.19), we regard $e_i \in [0,1]$ and $e_a \in \mathbb{R}_+$ as parametric coordinates. Note that the explicit expressions for $\widetilde{\Gamma}_1$ and $\widetilde{\Gamma}_2$, are not necessary, except that $\widetilde{\Gamma}_1 = 0 = \widetilde{\Gamma}_2$, in the absence of infection. We then study the system with these parametric variables by simply writing q_i where in fact, $q_i = q_i(e_a)$ for $i \in \{1,3,6\}$, $q_i = q_i(e_a, e_i)$ for $i \in \{2,4,5\}$ and $q_7 = q_7(e_i)$, with

$$\begin{aligned} q_1(e_a) &= \frac{1}{1+p_0 e_a}, \quad q_2(e_a,e_i) = \rho_1(1+\rho_2 e_a)e_i, \\ q_3(e_a) &= \frac{1}{1+p_1 e_a}, \quad q_4(e_a,e_i) = \rho_3(1+\rho_4 e_a)e_i, \\ q_5(e_a,e_i) &= \rho_5(1+\rho_6 e_a)e_i, \quad q_6(e_a) = \frac{1}{1+p_2 e_a}, \\ q_7(e_i) &= \rho_7 e_i. \end{aligned} \tag{2.22}$$

Each of the functions q_i, where $q_i : \mathbb{R}_+^2 \to \mathbb{R}_+$ for $i \in \{1,3,6\}$ and $q_i : \mathbb{R}_+ \to \mathbb{R}_+$ for $i \in \{2,4\}$, are positive monotone functions that measure the effect of adaptive and innate immunity in the different aspects of the within human host dynamics of the malaria parasite as explained in the derivation of the model in Refs. 22 and 29. In this rendition, we see immediately that q_1, q_3 and q_6 are monotone decreasing functions of the adaptive immunity function $e_a(t)$ while q_2, q_4, q_5 and q_7 are monotone increasing functions of the adaptive and innate immunity functions $e_a(t)$ and $e_i(t)$. We have the following bounds on the different functions:

$q_1(e_a)$, $q_3(e_a)$ and $q_6(e_a)$: The adaptive immune response e_a is zero in the absence of infection and kicks in when infection is present, and thereafter wanes away to zero when the infection is removed or cleared. Thus, $e_a(t) \geq 0$, $\forall t \geq 0$. We expect $\inf_{e_a}\{q_1(e_a)\} > 0$, since the adaptive immune response cannot continue to increase indefinitely. Therefore, we have $0 < q_1, q_3, q_6 \leq 1$ for all $t \geq 0$.
$q_2(e_a,e_i)$, $q_4(e_a,e_i)$, $q_5(e_a,e_i)$ and $q_7(e_i)$: In the context of the scaling done in this paper, the innate immunity response $e_i(t)$ can vary from $e_i(t) = 0$, complete immune depletion and deficiency, to maximum operability $e_i(t) = 1$. Thus, combined with the fact that e_a increases from zero, we have the bounds $0 < q_2 < \rho_1(1+\rho_2 \sup_{e_a} e_a)$, $0 < q_4 < \rho_3(1+\rho_4 \sup_{e_a} e_a)$, $0 < q_5 < \rho_5(1+\rho_6 \sup_{e_a} e_a)$ and $0 < q_7 < \rho_7$. Since $e_a = 0$ in the absence of infection and kick-starts in the presence of infection, the least upper bounds for q_2, q_4, q_5 and q_7 are, respectively, ρ_1, ρ_3, ρ_5 and ρ_7 occurring when $e_a = 0$.

With these parameter groupings for the system explicitly studied, system (2.13)–(2.17) then takes the form

$$\frac{dr_h}{d\tau} = a_0 g(r_h) - a_1 q_1 m r_h, \tag{2.23}$$

$$\frac{dr_p}{d\tau} = a_1 q_1 m r_h - (1+q_2) r_p, \tag{2.24}$$

$$\frac{dm}{d\tau} = a_2[q_3(1-\sigma) r_p - q_1(r_h + \beta r_p)m] - (a_3 + q_4)m, \tag{2.25}$$

$$\frac{dg_e}{d\tau} = a_4[q_3 \sigma r_p - g_e] - q_5 g_e, \tag{2.26}$$

$$\frac{dg_l}{d\tau} = a_5[q_6 g_e - g_l] - q_7 g_l. \tag{2.27}$$

Next, for given r_p and m values, all we need do is establish that Eqs. (2.18) and (2.19) have bounded solutions, if we desire to obtain an immune state for the human individual in question. From (2.18) and (2.19), it is clear that in the absence of infection, $\frac{de_i}{d\tau} = h(e_i) \Rightarrow e_i(t) = e_i(0) + \int_0^t h(e_i(s)ds$, for the forms of h in (2.21), and $\frac{de_a}{d\tau} = -c_6 e_a \Rightarrow e_a(t) = e_a(0)e^{-c_6 t}$.

In what follows next, we examine system (2.23)–(2.27) where e_a and e_i are parametric coordinates and the rest of the parameters are as stated. Note that the explicit forms of the system that model e_i and e_a as defined by Eqs. (2.18) and (2.19) are not necessary for our analysis, henceforth. To begin, we start by deriving the parasitemia reproduction number.

3. The Parasitemia Reproduction Number in Immune Presence

In this section, we briefly examine how the presence of an immune response can affect the intensity of propagation of merozoite transmission within the healthy red blood cell population by calculating and studying the effect of the immunity-based variables on the size of the parasitemia reproduction number for our full system. For within-human host malaria parasite dynamics, we treat the HRBCs as the susceptible population and the IRBCs as the infected population, with the merozoite population the infecting agent. Through this compartmentalization (see Fig. 1), we can then define *parasitemia reproduction number*, and use it as a measure of the strength or intensity of the force with which merozoites invade and destroy the healthy red blood cell population within the human at the onset of parasitemia. This measurable index points to whether or not parasitemia (systematic destruction of healthy red blood cells) will persists. Typically, if $\mathscr{R}_0 < 1$, each infected red blood cell eventually leads to the production, on average, less than one new infected red blood cell, indicating the possibility of controlling parasitemia at some point. However, if $\mathscr{R}_0 > 1$, then there is persistence of parasitemia.

Following our work in Ref. 29, it can be shown that

$$\mathscr{R}_0 = \varrho(FV^{-1}) = \frac{a_1 a_2 q_1 q_3 (1-\sigma)}{(q_2+1)(a_2 q_1 + a_3 + q_4)}, \tag{3.1}$$

where $(F)_{ij} = \frac{\partial \mathcal{F}_i}{\partial x_j}$ is the matrix of newly parasitized RBCs and $(V)_{ij} = \frac{\partial \mathcal{V}_i}{\partial x_j}$ are transfer terms, with

$$\mathcal{F}(\boldsymbol{x}) = \begin{pmatrix} 0 \\ a_1 m q_1 r_h \\ 0 \\ 0 \\ 0 \end{pmatrix},$$

$$\mathcal{V}(\boldsymbol{x}) = \begin{pmatrix} a_1 m q_1 r_h - a_0 g(r_h) \\ (q_2+1) r_p \\ m(a_3+q_4) - a_2(q_3 r_p (1-\sigma) - m q_1 (r_h + \beta r_p)) \\ g_e q_5 - a_4(q_3 r_p \sigma - g_e) \\ g_l q_7 - a_5(g_e q_6 - g_l) \end{pmatrix},$$

the matrices evaluated at the disease-free equilibrium, $\boldsymbol{x}_f^* = (1,0,0,0,0)^T$. Here, $\varrho(FV^{-1})$ is the spectral radius of the next generation matrix FV^{-1} (see Ref. 57).

Remark 1 (On the Parasitemia Reproduction Number in Immune Presence). The expression for $\mathscr{R}_0$ as defined by equation (3.1) is exactly the same expression associated with the conditions for the existence of a positive merozoite steady state, whereby for $\mathscr{R}_0 \leq 1$ there is no positive merozoite steady state population, and the only steady state is the parasite-free steady state. Details of this derivation can be found in Ref. 22. Additionally, the expression for $\mathscr{R}_0$ remains unchanged if we constructed the next generation matrix by considering only the disease terms.

A quick examination of the formula (3.1) as a function of $e_i \in [0,1]$ and $e_a \in \mathbb{R}_+$ and noting the behaviors of the quantities q_i as monotone functions of e_i and e_a, shows that the effect of the action of immunity on the system is to reduce the size of parasitemia reproduction number. In fact, from the form of $\mathscr{R}_0$, given that q_1 and q_3 are monotone decreasing functions of e_a while q_2 and q_4 are monotone increasing functions of e_a and e_i, the combined increased action of immune responses, will lead to a reduction overall size of $\mathscr{R}_0$. In particular, we have

$$\mathscr{R}_0 = \underbrace{\frac{a_1 a_2 q_1 q_3 (1-\sigma)}{(q_2+1)(a_2 q_1 + a_3 + q_4)}}_{\text{active } e_a>0 \text{ and } e_i \in (0,1)} \leq \underbrace{\frac{a_1 a_2 (1-\sigma)}{(1+\rho_1)(a_2+a_3+\rho_3)}}_{e_a=0, e_i=1} \leq \underbrace{\frac{a_1 a_2 (1-\sigma)}{(a_2+a_3)}}_{e_a=0, e_i=0}. \tag{3.2}$$

The inequality given by formula (3.2) simply expresses the fact that $\mathscr{R}_0$ increases with decreasing effectiveness of the immune response and attains a maximum value. It also captures the expectation that as the adaptive immunity kicks into action following repeated parasitemia, the actual value of the parasitemia reproduction number will continue to reduce in size. These two observations highlight the combined effects of these immunity-based responses in reducing the value of $\mathscr{R}_0$, thereby reducing the strength of parasitization of the red blood cells. The results also indicate that even in the absence of immune response, the parasitemia reproduction number can be bounded, which assures us that malaria parasitemia control is possible, even though $\mathscr{R}_0$ can continue to increase with increasing a_1. We shall investigate these further below as we continue to view the introduction of immunity into the system as a parameter into the system defined by Eqs. (2.13)–(2.19). The parameterized parameter $\mathscr{R}_0$ so identified can be used to study the behavior of the system in the presence of immunity.

4. Existence and Stability of Equilibrium Solutions

4.1. *Existence of equilibrium solutions*

To appreciate the effect of immunity on the system especially, on the eventual size of the steady state solutions and on the reproduction number, we now proceed to characterize the steady state solution on the above system in parametric form, that is in terms of two parameters $e_i \in [0,1]$ and $e_a \in \mathbb{R}^+$. Let $\boldsymbol{E}_{r_h^*} = (r_h^*, r_p^*(r_h^*), m^*(r_h^*), g_e^*(r_h^*), g_l^*(r_h^*))$ be a steady state solution, then as usual, setting the time derivatives to zero in (2.23)–(2.27) we find that

$$r_p^*(r_h^*) = \frac{a_0 g(r_h^*)}{q_2+1}, \tag{4.1}$$

$$m^*(r_h^*) = \frac{a_0(q_2+1)\mathscr{R}_0(a_2q_1+a_3+q_4)g(r_h^*)}{a_1q_1(a_2q_1(a_0\beta g(r_h^*)+q_2r_h^*+r_h^*)+a_3(q_2+1)+q_4(q_2+1))}, \tag{4.2}$$

$$g_e^*(r_h^*) = \frac{\sigma q_3 a_4}{a_4+q_5} r_p^*(r_h^*) = \frac{a_0 a_4 q_3 \sigma g(r_h^*)}{(q_2+1)(a_4+q_5)}, \tag{4.3}$$

$$g_l^*(r_h^*) = \frac{q_6 a_5}{a_5+q_7} g_e^*(r_h^*) = \frac{a_0 a_4 a_5 q_3 q_6 \sigma g(r_h^*)}{(q_2+1)(a_4+q_5)(a_5+q_7)}, \tag{4.4}$$

where $g(r_h)$ satisfies the equation $a_0 g(r_h^*) - a_1 q_1 m^*(r_h^*) r_h^* = 0$ leading to two solutions

$$\begin{aligned}(a)\ g(r_h^*) = 0 \text{ or } (b)\ g(r_h^*) \\ = \frac{(q_2+1)(a_2q_1(\mathscr{R}_0-1)r_h^*+(a_3+q_4)(\mathscr{R}_0 r_h^*-1))}{a_0a_2\beta q_1} = A_1 r_h^* - A_0,\end{aligned} \tag{4.5}$$

where

$$A_1 = \frac{(q_2+1)(a_2q_1(\mathscr{R}_0-1)+\mathscr{R}_0(a_3+q_4))}{a_0a_2\beta q_1},$$
$$A_0 = \frac{(q_2+1)(a_3+q_4)}{a_0a_2\beta q_1}, \tag{4.6}$$

and $\mathscr{R}_0 = \mathscr{R}_0(e_a^*, e_i^*)$ is given by (3.1). Note that A_0 and A_1 satisfy the following properties: (i) $A_0 > 0$ always, (ii) $0 < A_0 \leq A_1$ whenever $\mathscr{R}_0 > 1$ and (iii) more generally, $A_1 > 0$ for $\mathscr{R}_0 > \frac{a_2q_1}{a_2q_1+a_3+q_4}$, a value less than 1. From the definition of $\mathscr{R}_0$ in (3.1), the inequality in (iii) is true when $(1-\sigma)a_1q_3 > 1+q_2$.

The two equations for $g(r_h^*)$ given by (a) and (b) in (4.5) provide a pathway to obtaining all the steady state values, r_h^*, for the different types of recruitment functions as follows: By construction, $g : [0,\infty) \to \mathbb{R}$ is either a strictly monotone decreasing function of r_h with $g(1) = 0$ or a unimodal (one hump) continuously differentiable function of r_h with $g(0) = g(1) = 0$, so that by Rolle's theorem there exist $r_h^m \in (0,1)$ such that $g'(r_h^m) = 0$. Thus $g(r_h) \leq g(r_h^m)$ for all r_h. That is the equation $g(r_h) = 0$ has at most two solutions for all forms of $g(r_h)$ allowed by Definition 1. We deduce that $g(r_h)$ is monotone decreasing for all values of $r_h > r_h^m$ and monotone increasing for $0 \leq r_h < r_h^m$. So the equation $g(r_h) = A_1r_h - A_0$ can have exactly one solution that will occur at the point where the strictly monotone increasing function $y(r_h) = A_1r_h - A_0$ meets the function $y(r_h) = g(r_h)$, for $r_h > r_h^m$ or $r_h \in [0, r_h^m)$, the two intervals where g is strictly monotone. Whether or not the solution identified from here is realistic in the sense of the scaling done in this paper will be determined by the parameters of the system. Notice that as $\mathscr{R}_0$ increases from 0, A_1 also increases and so the two curves defined by $g(r_h)$ and $A_1r_h - A_0$ must meet at some point in the right-half plane where $r_h \geq 0$, and there exists parameter values for which the curves meet for $r_h \in [0,1]$. So not all solutions of the equation $g(r_h) = A_1r_h - A_0$ are admissible solutions. We have the following definition.

Definition 3. A solution $r_h^* \in \mathbb{R}$ of the equation $g(r_h^*) = 0$ or $g(r_h^*) = A_1r_h^* - A_0$ is said to be realistic, that is acceptable within the delimitations set by the scaling in this paper, if it is non-negative and bounded and $0 \leq r_h^* \leq 1$.

In Fig. 3(a), when $\mathscr{R}_0 < 1$, the intersection point of $g(r_h)$ and $A_1r_h - A_0$, occurs at negative values of the growth functions and the value of r_h at which the intersection occurs is greater than 1. No parasitized steady state exists for this case; only the parasite-free (or merozoite-free) steady state, in addition to the trivial steady state for the more nonlinear birth rate functions. In Fig. 3(b), with $\mathscr{R}_0 = 1$, only the parasite-free steady state in addition to the trivial steady state for the nonlinear functions exist. As $\mathscr{R}_0$ increases further from unity, we now have two steady states for the linear recruitment function, the parasite-free and a parasitized steady state, and three for the nonlinear $g(r_h)$ functions, the two mentioned and the trivial steady state. Additionally, $r_h^* \to 0$ as $\mathscr{R}_0 \to \infty$ as illustrated in figures

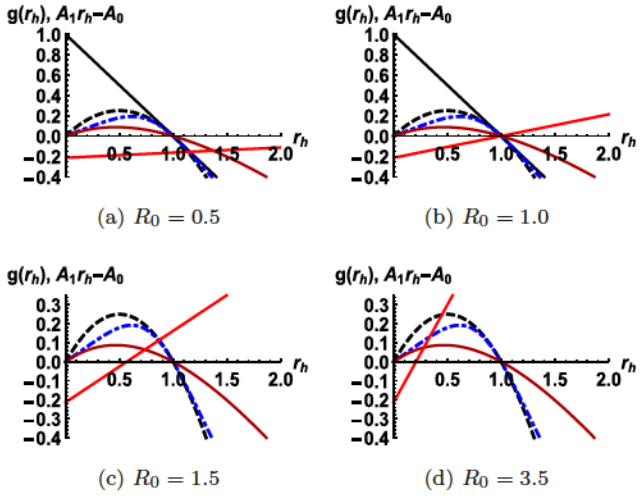

Fig. 3. Figure showing the existence of steady states as $\mathscr{R}_0$ increases through unity in relation to all forms of recruitment functions. The solid red increasing graph represents the curve for $A_1 r_h - A_0$, meanwhile the remaining curves represent $g(r_h)$ for the four types of recruitment functions studied. The solid black decreasing curve represents the linear recruitment function; the black dashed curve the logistic; the blue dot-dashed curve the Ricker and the solid dark red curve the Maynard–Smith–Slatkin recruitment function as described in Sec. 2.2 and shown in non-dimensional forms in Eq. (2.20). In (a), $\mathscr{R}_0 < 1$ and the red increasing curve intersect $g(r_h)$ for values of $r_h > 1$ where the growth functions are negative, and there is no parasitized steady state. In (b), $\mathscr{R}_0 = 1$ and the intersection is at $r_h = 1$, giving the parasite-free steady state and no parasitized steady state. For $\mathscr{R}_0 > 1$, the intersection is for r_h values between 0 and 1; graphs (c) and (d). As $\mathscr{R}_0$ further increases from unity, the intersection point shifts progressing toward smaller values of r_h; (c) and (d). In general, $r_h^* \to 0$ as $\mathscr{R}_0 \to \infty$ as explained in the text.

indicates that the size of the parasitized steady states is decreasing for increasing $\mathscr{R}_0$. This makes sense as large $\mathscr{R}_0$ values are associated with heavy parasitemia. The mathematical details associated with existence of steady states are explained in the text below.

Restricting ourselves to solutions that satisfy Definition 3, we consider existence of steady state solutions case by case, as each case is determined by the type of recruitment function being considered.

Case 1: $g(r_h) = 1 - r_h$, this is the case of linear recruitment linear death model. We have the following:

(a) $g(r_h^*) = 0 \Rightarrow r_h^* = 1$ is the unique steady state solution. When this steady state solution for r_h^* is substituted into (4.2)–(4.4), it leads to the steady state solution $E_{r_h^*=1} = (1, 0, 0, 0, 0)$. This is the disease-free, or merozoite-free steady state solution which we denote by $\boldsymbol{x}_f$.

(b) In the second instance, we have $g(r_h^*) = A_1 r_h^* - A_0$, and so to get the steady solution we must solve the equation $1 - r_h^* = A_1 r_h^* - A_0$, giving the solution $r_h^* = \frac{1+A_0}{1+A_1}$. Since $0 < A_0 \leq A_1$ whenever $\mathscr{R}_0 \geq 1$, $r_h^* \in (0, 1]$. r_h^* so obtained

is the only realistic parasitized steady state solution. To see this, we use the expressions for A_1 and A_0 defined by (4.6) and observe that the expression $A_1 r_h - A_0$ may be rearranged in the form

$$\begin{aligned} A_1 r_h - A_0 &= \left(\frac{(1+q_2)(a_2 q_1 + a_3 + q_4)(\mathscr{R}_0 - 1)}{a_0 a_2 \beta q_1} + A_0 \right) r_h - A_0, \\ &= \left(\frac{(1+q_2)(a_2 q_1 + a_3 + q_4)(\mathscr{R}_0 - 1)}{a_0 a_2 \beta q_1} \right) r_h + A_0(r_h - 1). \end{aligned}$$

Thus, when $\mathscr{R}_0 < 1$, $A_1 r_h - A_0 < 0$ whenever $r_h < 1$ indicating that there are no positive values of $r_h \in (0,1)$ such that $1 - r_h = A_1 r_h - A_0$ for this range of values of $\mathscr{R}_0$. When $\mathscr{R}_0 = 1$, $A_1 = A_0$ and we have the solution $r_h^* = 1$ leading back to the merozoite free steady state solution x_f^*. If $\mathscr{R}_0 > 1$, $r_h^* \in (0,1)$ and when this value of r_h^* is substituted into (4.2)–(4.4), it leads to the parasitized steady state solution. In this second case, the parametric equations for the steady state may be explicitly written. That is, for the parameters $e_i \in [0,1]$ and $e_a \in [0,\infty)$, we have

$$r_h^*(e_a^*, e_i^*) = \frac{a_0 a_2 \beta q_1^* + (a_3 + q_4^*)(q_2^* + 1)}{a_2 q_1^*(a_0\beta + (q_2^*+1)(\mathscr{R}_0 - 1)) + (q_2^*+1)\mathscr{R}_0(a_3 + q_4^*)},$$

$$r_p^*(e_a^*, e_i^*) = \frac{a_0(a_2 q_1^* + a_3 + q_4^*)(\mathscr{R}_0 - 1)}{a_2 q_1^*(a_0\beta + (q_2^*+1)(\mathscr{R}_0 - 1)) + (q_2^*+1)\mathscr{R}_0(a_3 + q_4^*)},$$

$$m^*(e_a^*, e_i^*) = \frac{a_0(q_2^*+1)(a_2 q_1^* + a_3 + q_4^*)(\mathscr{R}_0 - 1)}{a_1 q_1^*(a_0 a_2 \beta q_1^* + a_3(q_2^*+1) + (q_2^*+1)q_4^*)},$$

$$g_e^*(e_a^*, e_i^*) = \frac{a_0 a_4 q_3^* \sigma (a_2 q_1^* + a_3 + q_4^*)(\mathscr{R}_0 - 1)}{(a_4 + q_5^*)(a_2 q_1^*(a_0\beta + (q_2^*+1)(\mathscr{R}_0 - 1)) + (q_2^*+1)\mathscr{R}_0(a_3 + q_4^*))},$$

$$g_l^*(e_a^*, e_i^*) = \frac{a_0 a_4 a_5 q_3^* q_6^* \sigma (a_2 q_1^* + a_3 + q_4^*)(\mathscr{R}_0 - 1)}{(a_4 + q_5^*)(a_5 + q_7^*)(a_2 q_1^*(a_0\beta + (q_2^*+1)(\mathscr{R}_0 - 1)) + (q_2^*+1)\mathscr{R}_0(a_3 + q_4^*))},$$

where $q_i^* = q_i(e_a^*, e_i^*)$ are the immune functions defined by (2.22).

Case 2: $g(r_h) = r_h(1 - r_h)$. This is the case of the logistic recruitment growth model.

(a) $g(r_h^*) = 0 \Rightarrow r_h^*(1 - r_h^*) = 0$. We now have two solutions: $r_h^* = 0$ or $r_h^* = 1$. The steady state solution $r_h^* = 0$ leads to the trivial steady state solution $E_{r_h^*=0} = (0,0,0,0,0)$ while the steady state solution $r_h^* = 1$ again produces the merozoite-free steady state solution $E_{r_h^*=1} = (1,0,0,0,0)$.

(b) $g(r_h^*) = A_1 r_h^* - A_0 \Rightarrow r_h^*(1 - r_h^*) = A_1 r_h^* - A_0$, which upon solving the quadratic equation and noting that $A_0 > 0$ always, with $A_1 > 0$ and $A_0 \leq A_1$ whenever $\mathscr{R}_0 \geq 1$, yield the solutions $r_h^* = \frac{1}{2}((1 - A_1) \pm \sqrt{(1 - A_1)^2 + 4A_0})$, and we retain

the positive solution for r_h^*, whose existence in the interval $(0,1)$ is illustrated by Fig. 3. It is however easy to verify that since $A_0 \leq A_1$ whenever $\mathscr{R}_0 \geq 1$, $0 < r_h^* = \frac{1}{2}((1-A_1) + \sqrt{(1-A_1)^2 + 4A_0}) < 1$. When this solution for r_h^* is substituted into (4.2)–(4.4), it yields the corresponding parasitized state for the logistic recruitment function, in parametric form where the parameter here are the variables $e_i \in [0,1]$ and $e_a \in [0,\infty)$ as earlier explained, and the exact steady state is given by

$$\begin{aligned} r_h^* &= \frac{1}{2}((1-A_1) + \sqrt{(1-A_1)^2 + 4A_0}) \\ &= \frac{2A_0}{A_1 - 1 + \sqrt{(1-A_1)^2 + 4A_0}}, \\ r_p(r_h^*) &= \frac{a_2 q_1(\mathscr{R}_0 - 1) r_h^* + (a_3 + q_4)(\mathscr{R}_0 r_h^* - 1)}{a_2 \beta q_1}, \\ m^*(r_h^*) &= \frac{(q_2+1)(a_2 q_1(\mathscr{R}_0 - 1) r_h^* + (a_3 + q_4)(\mathscr{R}_0 r_h^* - 1))}{a_1 a_2 \beta q_1^2 r_h^*} \\ &= \frac{(1+q_2) r_p^*(r_h^*)}{a_1 q_1 r_h^*}, \\ g_e^*(r_h^*) &= \frac{\sigma a_4 q_3}{(a_4 + q_5)} r_p^*(r_h^*), \quad g_l^*(r_h^*) = \frac{a_5 q_6}{a_5 + q_7} \frac{\sigma a_4 q_3}{(a_4 + q_5)} r_p^*(r_h^*) \end{aligned} \tag{4.7}$$

and the steady states are completely computed for this birth rate function.

Case 3: $g(r_h) = r_h e^{\ln(\mu) r_h} - \mu r_h$. This is the case for the Ricker recruitment model.

(a) $g(r_h^*) = 0$: That is $r_h^* e^{\ln(\mu) r_h^*} - \mu r_h^* = 0$. This leads to the solution $r_h^* = 0$ or $r_h^* = 1$. As before, the solution $r_h^* = 0$ leads to the trivial steady state solution $E_{r_h^*=0} = (0,0,0,0,0)$ and the steady state $r_h^* = 1$ leads to the merozoite-free steady state $\boldsymbol{x}_f = (1,0,0,0,0)$.

(b) When $g(r_h^*) = A_1 r_h^* - A_0$, we have to find a solution for the nonlinear equation $r_h^* e^{\ln(\mu) r_h^*} - \mu r_h^* = A_1 r_h^* - A_0$. At this point, we immediately hit a snag seeing that the solution procedure is no longer straight forward. However, we note that when a realistic solution exists, it occurs at the point where the straight line defined by the equation $y(r_h^*) = A_1 r_h^* - A_0$ and the curve $y(r_h^*) = r_h^* e^{\ln(\mu) r_h^*} - \mu r_h^*$ meet, as illustrated in Fig. 3. Such a solution $r_h^* \leq 1$ exists only when $\mathscr{R}_0 > 1$. To see this analytically, define $S(r_h^*) = r_h^* e^{\ln(\mu) r_h^*} - \mu r_h^* - A_1 r_h^* + A_0$. Then clearly $S : [0,\infty) \to \mathbb{R}$ is a continuous function of r_h^* with $S'(r_h^*) < 0$ whenever $r_h^* \geq 0$ and $S'(0) = 1 - \mu - A_1 \leq 0$ whenever $\mathscr{R}_0 > 1$. Note that $S(\frac{A_0}{A_1}) > 0$ and $S(1) < 0$. Thus, we can use the intermediate value theorem to say with certainty that there exist r_h^*, with $\frac{A_0}{A_1} < r_h^* < 1$ such that $g(r_h *) = A_1 x^* - A_0$. The solution r_h^* so bracketed is uniquely determined.

Case 4: $g(r_h) = r_h\left(1 + \left(\frac{1}{\mu} - 1\right)r_h^n\right)^{-1} - \mu r_h$. This is the Maynard–Smith–Slatkin growth rate model reducible to the Beverton–Holt when $n = 1$. Two cases just as above are treatable:

(a) $g(r_h^*) = 0$: That is $r_h\left(1 + \left(\frac{1}{\mu} - 1\right)r_h^n\right)^{-1} - \mu r_h = 0$. This leads to the solution $r_h^* = 0$ or $r_h^* = 1$. As before, the solution $r_h^* = 0$ leads to the trivial steady state solution $E_{r_h^*=0} = (0, 0, 0, 0, 0)$. Second, the steady state $r_h^* = 1$ leads to the merozoite free steady state solution $\boldsymbol{x}_f = (1, 0, 0, 0, 0)$.

(b) When $g(r_h^*) = A_1 r_h^* - A_0$, we have to obtain r_h^* through the nonlinear equation $r_h^*\left(1 + \left(\frac{1}{\mu} - 1\right)r_h^{*n}\right)^{-1} - \mu r_h^* = A_1 r_h^* - A_0$. Again, we hit a snag with a solution procedure that is no longer straight forward. However we notice that when a solution exists, it occurs at the point where the straight line defined by the equation $y(r_h^*) = A_1 r_h^* - A_0$ and the nonlinear curve $y(r_h^*) = r_h^*\left(1 + \left(\frac{1}{\mu} - 1\right)r_h^{*n}\right)^{-1} - \mu r_h^*$ meet. Such a solution $0 < r_h^* < 1$ exists only when whenever $\mathscr{R}_0 > 1$ as illustrated in Fig. 3. To see this analytically, define the nonlinear function $S(r_h)$ by $S(r_h) = r_h\left(1 + \left(\frac{1}{\mu} - 1\right)r_h^n\right)^{-1} - \mu r_h - A_1 r_h + A_0$. Then clearly $S : [0, \infty) \to \mathbb{R}$ is a continuous function of r_h with $S'(r_h) = -A_1 + \frac{1-(n-1)\left(\frac{1}{\mu}-1\right)r_h^n}{\left(1+\left(\frac{1}{\mu}-1\right)r_h^n\right)^2} - \mu$. Observe that when $\mathscr{R}_0 > 1$, $n > 1$ and considering the range of values of r_h^* in the feasible region, namely $0 \le r_h^* \le 1$, $S'(r_h^*) < 0$, so that $S : \mathbb{R}^+ \to \mathbb{R}$ is monotone decreasing, indicating that when a solution r_h^* for $S(r_h^*) = 0$ exist, it is uniquely determined. From the sizes of the parameter groupings and the definition of S, we find that $S(\frac{A_0}{A_1}) > 0$ and $S(1) < 0$. Thus, we can use the intermediate value theorem to say with certainty that there exist r_h^*, with $\frac{A_0}{A_1} < r_h^* < 1$ such that $g(r_h*) = A_1 x^* - A_0$. The solution r_h^* so bracketed is uniquely determined whenever $\mathscr{R}_0 > 1$.

Clearly $\mathscr{R}_0$ as defined by (3.1) uniquely determines the existence and size of the parasitized state defined by the equation $g(r_h^*) = A_1 r_h^* - A_0$ in that a solution $r_h^* \in (0, 1)$ exists only when $\mathscr{R}_0 > 1$. Closer examination of the expression for $\mathscr{R}_0$ and noting that $0 < q_1, q_3 < 1 \ \forall \ \ e_a > 0$, we find that

$$\begin{aligned}\mathscr{R}_0(e_a^*, e_i^*) &= \frac{a_1 a_2(1-\sigma)}{(1+\rho_1 e_a^*)(1+q_2^*)(a_2 + (1+p_0 e_a^*)(a_3+q_4^*))} \\ &< a_1(1-\sigma) \le a_1. \end{aligned} \tag{4.8}$$

Thus, we can regard an increase in a_1 as an increase in the upper bound of the parasitemia reproduction number $\mathscr{R}_0$. From the forgoing we have proved the following result.

Theorem 1 (On the existence of the steady state solutions). *Let $e_i \in [0, 1]$ and $e_a \in \mathbb{R}^+$ be parametric coordinates. Let functions $q_i : [0, 1] \times \mathbb{R}^+ \to \mathbb{R}^+$ be as defined in* (2.22). *Then system* (2.23)–(2.27) *has at least one realistic steady state solution for every suitable form of the recruitment function $g(r_h)$. In particular,*

the parasite-free steady state $(1,0,0,0,0)$ *always exists for all forms of the recruitment function* g *considered and a realistic parasitized steady state solution also exist whenever a uniquely determined threshold parameter* $\mathscr{R}_0 > 1$. *In this case, the value of the parasitized steady state can be uniquely determined in terms of the immunity variables as parametric coordinates.*

4.2. *Some properties of the equilibrium solutions*

The size of the parasitized state predicted by Theorem 1 is completely determined by the parameters of the system in the sense that as $\mathscr{R}_0$ increases from 0 the only non-trivial steady state solution is the merozoite free steady state. However, as $\mathscr{R}_0$ increases further through the value unity, the destruction of the healthy red blood cells through parasitization begins and the size of the steady state solution for the red blood cells begin to decrease as the size of the steady state for the merozoite population starts increasing from zero. However, as more and more red blood cells get parasitized, there will come a time when there is a depleted red blood cell density, and so, then, we expect the merozoite population steady state to start decreasing for further increases in $\mathscr{R}_0$. We state the following result.

Lemma 1. *Let* $g : [0,\infty) \longrightarrow \mathbb{R}$ *be a recruitment function for system* (2.13)–(2.17). *Let* $\mathscr{R}_0 > 0$ *be defined by* (3.1) *with respect to the scaled immunity-based state variables* e_a *and* e_i. *Let* $r_h^* \in (0,1)$ *be a realistic steady state solution for system* (2.13)–(2.17), *that satisfies the equation* $g(r_h^*) = A_1 r_h^* - A_0$, *where* A_1 *and* A_0 *are defined by* (4.6). *Then* $\lim_{\mathscr{R}_0 \to \infty} r_h^*(\mathscr{R}_0) = 0$ *whenever* $A_1 > g'(r_h)$.

Proof. By construction of g, $g(1) = 0$ and $g'(r_h) < 0$ for $r_h^m < r_h \leq 1$. Also from the definition of A_1 and A_0 we have $g(r_h^*) = A_1 r_h^* - A_0$ with $A_1 > 0$ whenever $\mathscr{R}_0 > 1$. Therefore implicit differentiation yields

$$\frac{dr_h^*}{d\mathscr{R}_0} = -\frac{r_h^*}{A_1 - g'(r_h^*)} \frac{dA_1}{d\mathscr{R}_0} < 0 \quad \text{whenver } A_1 > g'(r_h^*).$$

Thus r_h^* is ever decreasing as a function of $\mathscr{R}_0$ and as such, in the limit as A_1 becomes very large for large values of $\mathscr{R}_0$, $r_h^* \to 0$, as required. □

Lemma 2. *Let* $g : [0,\infty) \to \mathbb{R}$ *be a recruitment function for system* (2.13)–(2.17). *Let* $\mathscr{R}_0 > 0$ *be defined by* (3.1) *with respect to the scaled immunity-based state variables* e_a *and* e_i. *Let* $r_h^* \in (0,1)$ *be a realistic steady state solution for system* (2.13)–(2.17), *that satisfies the equation* $g(r_h^*) = A_1 r_h^* - A_0$, *where* A_1 *and* A_0 *are defined by* (4.6). *Then the corresponding steady state values for* $m^*(r_h^*)$ *and* $r_p^*(r_h^*)$ *as defined by* (4.1) *and* (4.2) *are bounded and their bounds are completely determined by the form the function* $g : [0,\infty) \to \mathbb{R}$.

Proof. For a given function $g : [0,\infty) \to \mathbb{R}$ satisfying Definition 1, the steady state density $r_p^*(r_h^*)$ is given by (4.1). Now, from the definition of g, we have that

either $g(0) = 1$ and $g(1) = 0$ in the case of the linear recruitment function, or $g(0) = g(1) = 0$ in the case of the other recruitment functions. In the case of the linear recruitment function, $0 \leq g(r_h) \leq 1$ for all $r_h \in [0,1]$. For the other recruitment functions, from the continuity, differentiability and continuity of g on $[0,1]$, by Rolle's theorem, there exists $r_h^m \in (0,1)$ such that $g'(r_h^m) = 0$ and $g(r_h) \leq g(r_h^m), \forall r_h \in [0,1]$. So if $g_m = \max_{r_h \in [0,1]} g(r_h)$, then we have

$$r_p^*(r_h^*) = \frac{a_0}{1+q_2} g(r_h^*) \leq \frac{a_0}{1+q_2} g_m < a_0 g_m \quad \text{since } \frac{1}{1+q_2} < 1, \tag{4.9}$$

where for $r_h^m \in [0,1]$ satisfying the equation $g'(r_h^m) = 0$,

$$g_m = \begin{cases} 1 & \text{if } g(r_h) = 1 - r_h, \\ g(r_h^m) & \text{for } g(r_h) \text{ otherwise.} \end{cases} \tag{4.10}$$

The steady state value $m^*(r_h^*)$ is given by (4.2), which we write in the form

$$m^*(r_h^*) = \frac{m_1 g(r_h^*)}{m_2 g(r_h^*) + m_3 r_h^* + m_4}, \tag{4.11}$$

where

$$m_1 = a_0(q_2+1)\mathscr{R}_0(a_2 q_1 + a_3 + q_4), \quad m_2 = \beta a_0 a_1 a_2 q_1^2,$$
$$m_3 = a_1 a_2 q_1^2 (1+q_2), \quad m_4 = a_1 q_1 (a_3 + q_4)(1+q_2).$$

For the linear recruitment model, $g(r_h) = 1 - r_h$ is decreasing and we have $m^*(r_h^*) \leq m^*(0)$. For the other types of recruitment functions satisfying Definition 1, we have that $m^*(0) = m^*(1) = 0$ and so from positivity, differentiability and continuity of m, there exists $r_h^s \in (0,1)$ such that $m'(r_h^s) = 0$. That is $m^*(r_h)$ attains a maximum value for r_h in the interval $[0,1]$. We easily establish that at such a maximum point any admissible function $g : [0,\infty) \to \mathbb{R}$ should satisfy the first-order ordinary differential equation $g'(r_h) - \frac{m_3}{m_3 r_h + m_4} g(r_h) = 0$. Solving this differential equation for $g(r_h)$, leads to the solution $g(r_h) = \kappa(m_3 r_h + m_4)$, for some arbitrary constant $\kappa \geq 0$. This then leads to the maximum possible value of m^* given by

$$m^*(r_h^*) \leq \begin{cases} \dfrac{m_1}{m_2 + m_4} & \text{if } g(r_h) = 1 - r_h, \\ \dfrac{m_1 \kappa}{m_2 \kappa + 1} & \text{for } g(r_h) \text{ otherwise,} \end{cases} \tag{4.12}$$

where the constant κ, though arbitrary, must be chosen as the largest positive κ such that the equation $g(r_h) = \kappa(m_3 r_h + m_4)$ has real a positive solution $r_h \in [0,1]$. For example, for the logistic growth model where $g(r_h) = r_h(1-r_h)$, we need to find the maximum point by solving the equation $r_h(1-r_h) - \kappa(m_3 r_h + m_4) = 0$ for $r_h \in (0,1)$ and largest $\kappa > 0$. For this, it is sufficient to set $\kappa = \min_\kappa\{(1 - \kappa m_3)^2 - 4 m_4 \kappa = 0\} = \frac{m_3 + 2m_4 - 2\sqrt{m_4(m_3+m_4)}}{m_3^2}$. Similar values for κ for the other growth functions can be found. However, it is easy to actually see from the definition of m^* from (4.11) that $m^* < \frac{m_1}{m_2} = \frac{(1-\sigma)q_3}{\beta q_1}$, for all forms of recruitment functions. □

Remark 2. The inequality (4.9) shows that the *ultimate size* of the density of parasitized red blood cells at equilibrium is determined by the quantity of the red blood cell population in the first place (that is by maximum possible rate of recruitment of healthy red blood cells from the bone marrow), and not strongly dependent on the action of immunity. However, the presence of innate and adaptive immunity can reduce this maximum possible size by a quantifiable scale factor of $\frac{1}{1+q_2}$. This result points to the assertion that knowing the efficiency of the rate of recruitment of healthy red blood cells into the system is an important parameter in understanding the health status of the individual in case of management of anaemia.

Having obtained bounds for r_p^* and m^*, the bounds for g_e^* and g_l^* become evident since from (4.3) and (4.4) these are defined simply in terms of g and $g \leq g_m$. Now the bounds for the steady state variables r_p^*, m^*, g_e^* and g_l^* are defined in terms of immunity parameters e_i and e_a. From the scaling done in this paper, we have that $0 \leq e_i \leq 1$, where $e_i = 1$ is the optimum operational level for the innate immune response and $e_i = 0$ is the minimum or immune suppressed state as studied in Refs. 22 and 29. In this paper, we have allowed for the possibility of adaptive immunity to start acting once there is an infection in the system, and it is also stimulated by the action of the innate immune response. As adaptive immunity increases with sustained parasitemia it's ultimate equilibrium size is also bounded as we now demonstrate in the following result.

Lemma 3. *Assume that at equilibrium the immune effector cells as parameterized by e_a and by e_i satisfy* (2.18) *and* (2.19) *when the time derivatives are set to zero. Then at equilibrium, the immune variables e_a^* and e_i^* are also bounded and their bounds are completely determined for every admissible form of the recruitment function g.*

Proof. By construction, $0 \leq e_i \leq 1$ so e_i^* is always bounded. We therefore only need to show that within the limitations of the model derived in this paper, e_a^* is also bounded. From (2.19), at equilibrium we have

$$e_a^*(r_h) = \frac{r_p^*(r_h) + b_3 m^*(r_h)}{a_6 + c_3(r_p^*(r_h) + c_4 m^*(r_h))} \equiv E(r_h), \tag{4.13}$$

where we are only interested in those values of $r_h \in [0, 1]$ wherein a feasible steady state solution lies. From the values of $r_p^*(r_h)$ and $m^*(r_h)$ given in (4.1) and (4.2) and from the construction of g, if $g(r_h)$ is the linear recruitment function, then $0 \leq e_a^*(r_h) \leq E(0)$. If $g(r_h)$ is any of the nonlinear recruitment functions, then we have, $E(0) = E(1) = 0$, and from continuity and differentiability of g, there exist $r_h^{e_a} \in (0, 1)$ such that $E'(r_h^{e_a}) = 0$ and at which point we have $0 \leq e_a^*(r_h) \leq E(r_h^{e_a})$. That is $E(r_h)$ attains a global maximum at the point where $r_h = r_h^{e_a} \in (0, 1)$. Thus, the actual bound for e_a^* can be computed by solving the inequality $0 \leq e_a^* \leq E(0)$ for the linear recruitment function or the inequality $0 \leq e_a^* \leq E(r_h^{e_a})$ for the other recruitment functions, to obtain the exact estimates for the bounds of the adaptive

immune variable at equilibrium, namely, e_a^*. However, a larger estimate for the bound can be constructed by inserting the bounds for r_p^* and m^* given by (4.9) and (4.12) in (4.13) to have

$$E(r_h) = \frac{r_p^*(r_h) + b_3 m^*(r_h)}{a_6 + c_3(r_p^*(r_h) + c_4 m^*(r_h))} \leq \frac{r_p^*(r_h) + b_3 m^*(r_h)}{a_6} < \frac{a_0 g_m + \frac{m_1}{m_2}}{a_6}.$$

On substituting the values of m_1 and m_2 from (4.12), and rearranging, we find that an upper bound for e_a^*, e_a^∞, say, will satisfy the inequality

$$e_a^\infty < \frac{a_0 g_m + b_3 \frac{1-\sigma}{\beta} \frac{1+p_0 e_a^\infty}{1+p_1 e_a^\infty}}{a_6} \Rightarrow 0 \leq e_a^* < e_a^\infty \leq \frac{-e_1 + \sqrt{e_1^2 + 4e_0 e_2}}{2e_2}, \quad (4.14)$$

where g_m is given by (4.10) and

$$e_2 = a_6 \beta p_1, \quad e_1 = a_6 \beta - (a_0 \beta p_1 g_m + b_3 p_0 (1-\sigma)), \quad e_0 = b_3(1-\sigma) + a_0 \beta g_m.$$

This establishes the fact that e_a^* is bounded. □

Remark 3. The inequality (4.14) indicates that the bound for the adaptive immune response depends on g_m, the maximum size of the growth function, and that the bound becomes adjusted upwards whenever $\sigma < 1$. Thus the phenomenon of commitment of infected red blood cells, in the life cycle of the malaria bug, toward the gametocytogenesis path has a substantial effect on the strength of an adaptive immune response in a malaria positive patient.

4.3. *Stability of equilibrium solutions*

In this section, we discuss the stability of the computed equilibria or steady states starting with their linear stability properties. The linear stability of steady state solutions can be determined by calculating the eigenvalues of the Jacobian matrix at the respective steady states. We continue to use the parametric form of the system where the parametric coordinates are the innate and adaptive immune response variables.

Let $\boldsymbol{x} = (r_h, r_p, m, g_e, g_l)$ be a vector of the parameterized state variables. Let $J(\boldsymbol{x})$ be the Jacobian matrix of the system at the point $\boldsymbol{x}$. Then

$$J(\boldsymbol{x}) = \begin{pmatrix} a_0 g'(r_h) - m a_1 q_1 & 0 & -r_h a_1 q_1 & 0 & 0 \\ m a_1 q_1 & -q_2 - 1 & r_h a_1 q_1 & 0 & 0 \\ -m a_2 q_1 & B_1 - m\beta a_2 q_1 & -a_3 - B_2 - q_4 & 0 & 0 \\ 0 & a_4\left(q_3 - \frac{B_1}{a_2}\right) & 0 & -a_4 - q_5 & 0 \\ 0 & 0 & 0 & a_5 q_6 & -a_5 - q_7 \end{pmatrix} \quad (4.15)$$

where

$$B_1 = \frac{(q_2+1)(a_3 + a_2 q_1 + q_4)\mathscr{R}_0}{a_1 q_1}, \quad B_2 = (r_h + r_p \beta) a_2 q_1.$$

Now, let λ be an eigenvalue of J. Then λ is the solution of the equation $P_5(\lambda, \boldsymbol{x}^*) = 0$ where $\boldsymbol{x}^*$ is a steady state solution of the system and

$$P_5(\lambda, \boldsymbol{x}^*) = |\lambda \boldsymbol{I} - J(\boldsymbol{x}^*)| = (\lambda + a_5 + q_7)(\lambda + a_4 + q_5)P_3(\lambda, \boldsymbol{x}^*). \tag{4.16}$$

Here, $\boldsymbol{I}$ is the identity matrix of order five and

$$P_3(\lambda, \boldsymbol{x}^*) = \lambda^3 + P(\boldsymbol{x}^*)\lambda^2 + Q(\boldsymbol{x}^*)\lambda + R(\boldsymbol{x}^*), \tag{4.17}$$

where

$$\begin{aligned}
P(\boldsymbol{x}^*) &= -a_0 g'(r_h^*) + q_1(a_1 m^* + a_2(r_h^* + \beta r_p^*)) + a_3 + q_2 + q_4 + 1,\\
Q(\boldsymbol{x}^*) &= a_3(-a_0 g'(r_h^*) + a_1 m^* q_1 - (q_2 + 1)(\mathscr{R}_0 r_h^* - 1))\\
&\quad - a_0 g'(r_h^*)(a_2 q_1(r_h^* + \beta r_p^*) + q_2 + q_4 + 1)\\
&\quad + a_1 m^* q_1(a_2 \beta q_1(r_h^* + r_p^*) + q_2 + q_4 + 1)\\
&\quad + (q_2 + 1)(a_2 q_1(-\mathscr{R}_0 r_h^* + r_h^* + \beta r_p^*) + q_4(1 - \mathscr{R}_0 r_h^*)),\\
R(\boldsymbol{x}^*) &= a_1 m^* q_1((q_2 + 1)(a_2 \beta q_1 r_p^* + a_3 + q_4) - a_0 a_2 \beta q_1 r_h^* g'(r_h^*))\\
&\quad + a_0(q_2 + 1)g'(r_h^*)(\mathscr{R}_0 r_h^*(a_2 q_1 + a_3 + q_4)\\
&\quad - a_2 q_1(r_h^* + \beta r_p^*) - a_3 - q_4).
\end{aligned}$$

We note that $g'(r_h)$ appears in expressions for P, Q and R but not $g(r_h)$. We now consider the local stability of the steady state $\boldsymbol{x}^*$ and note that such a steady state will be stable to small perturbations if, by the Routh Hurwitz stability criteria, $P > 0, Q > 0, R > 0$ and $PQ - R > 0$. We consider each of the solution types in turn.

Theorem 2 (On the local instability of the trivial equilibrium solution). *Let $g : [0, \infty) \to \mathbb{R}$ be the scaled rate of recruitment of the population of healthy red blood cell as found in system (2.23)–(2.27). If $r_h^* = 0$ exists as an equilibrium solution arising from the solution of the equation $g(r_h^*) = 0$, then the trivial equilibrium solution $(r_h^*, r_p^*, m^*, g_e^*, g_l^*) = (0, 0, 0, 0, 0)$ also exists as an unstable equilibrium solution of system (2.23)–(2.27) for all parameter regimes.*

Proof. The existence of a solution $r_h^* = 0$, as a steady state solution of the system (2.23)–(2.27) in the absence of infection is possible for the cases where $g(r_h)$ is constructed from the logistic, Ricker or Maynard–Smith–Slatikin recruitment functions as demonstrated above, or any recruitment function g with the property that $g(0) = 0$. We then have the following: when $g(r_h)$ is constructed from the logistic function, $g'(0) = 1 > 0$ and when $g(r_h)$ is from either the Ricker or Maynard–Smith–Slatkin birth recruitment functions, $g'(0) = 1 - \mu > 0$ (since $\mu < 1$). In each of these cases, $P_3(\lambda, \boldsymbol{0})$ factorizes completely into the factors $(\lambda - a_0)(\lambda + 1 + q_2)(\lambda + a_3 + q_4)$ for the logistic case and into factors $(\lambda - a_0(1 - \mu))(\lambda + 1 + q_2)(\lambda + a_3 + q_4)$ for the other two cases. In each instance, there is the presence of a growing solution

with positive exponent being a multiplicative factor of a_0. That is the trivial steady state is always unstable to small perturbations whenever it exists. □

Theorem 3 (On the local stability of the merozoite-free equilibrium solution). *Let $g : [0, \infty) \to \mathbb{R}$ be the scaled rate of recruitment of the population of healthy red blood cell as found in system (2.23)–(2.27). The solution $r_h^* = 1$ always exist as an equilibrium solution arising from the solution of the equation $g(r_h^*) = 0$, for all forms of the recruitment function g, and therefore, the merozoite-free (parasite-free) equilibrium solution $\boldsymbol{x}_f^* = (r_h^*, r_p^*, m^*, g_e^*, g_l^*) = (1, 0, 0, 0, 0)$ also always exists as an equilibrium solution of system (2.23)–(2.27) and its stability properties are uniquely determined by the size of the threshold parameter $\mathscr{R}_0$ given by (3.1) in the sense that when $\mathscr{R}_0 > 1$, the steady state $\boldsymbol{x}_f^*$ is locally unstable to small perturbations and stable otherwise.*

Proof. From the construction of g, the equation $g(r_h^*) = 0$ always has the non-trivial solution $r_h^* = 1$, as a steady state solution in the absence of infection, and will have the same value $r_h^* = 1$ for all forms of $g(r_h)$ considered, so that $\boldsymbol{x}_f^* = (1, 0, 0, 0, 0)$ always exists as a steady state of the system as explained above. Given the subtle differences in each case, we treat each at a time.

(i) **The cases** $g(r_h) = 1 - r_h$ and $g(r_h) = r_h(1 - r_h)$: For these two cases, we both have $g'(1) = -1$. In both case again the polynomial $P_3(\lambda, (1, 0, 0, 0, 0))$ factorizes to $P_3 = (\lambda + a_0)(\lambda^2 + s_1\lambda + s_0)$ where $s_1 = a_2q_1 + a_3 + q_2 + q_4 + 1$, and $s_0 = -(q_2 + 1)(\mathscr{R}_0 - 1)(a_2q_1 + a_3 + q_4)$. Here, $\mathscr{R}_0$ is given by (3.1). Clearly, s_1, $s_0 > 0$ and $s_1^2 - 4s_0 > 0$ are all positive when $\mathscr{R}_0 < 1$ so that all zeroes of the polynomial P_3 will have negative real parts whenever $\mathscr{R}_0 < 1$. For $\mathscr{R}_0 = 1$, $\lambda = 0$ is one of the eigenvalues accompanied by two negative eigenvalues. On the other hand, as $\mathscr{R}_0$ increases through the value $\mathscr{R}_0 = 1$, $s_1 > 0$ and $s_0 < 0$ for $\mathscr{R}_0 > 1$ signifying the presence of growing perturbations with positive exponent. That is the steady state solution $(1, 0, 0, 0, 0)$ loses stability as $\mathscr{R}_0$ increases through unity, and is always stable when $\mathscr{R}_0 \leq 1$ for the logistic and linear cases.

(ii) **The cases** $g(r_h) = r_h e^{\ln(\mu)r_h} - \mu r_h$ and $g(r_h) = r_h(1 + (\frac{1}{\mu} - 1)r_h^n)^{-1} - \mu r_h$. In these cases again the polynomial $P_3(\lambda, (1, 0, 0, 0, 0))$ factorizes to $P_3 = (\lambda + \tilde{s}a_0)(\lambda^2 + s_1\lambda + s_0)$ where for the Ricker growth model, $\tilde{s} = -\mu \ln(\mu)$, for the Maynard–Smith–Slatkin growth model $\tilde{s} = -n\mu(\mu - 1)$ and s_1, s_0 retain the same forms as in the linear and logistic cases. Again, recalling that $0 < \mu \leq 1$ in both cases, $\tilde{s} > 0$ and the conclusion is thus the same: there are growing perturbations with positive exponent as $\mathscr{R}_0$ increases from 1 and the steady state solution $(1, 0, 0, 0, 0)$ loses stability as $\mathscr{R}_0$ increases through unity for the these types of birth function as well. □

In fact, it is easy to deduce that for any growth rate function for which $g(1) = 0$ and $g'(1) < 0$ as required by Definition 1, the dynamics will cause the steady state

$x_f^* = (1, 0, 0, 0, 0)$ to lose stability as $\mathscr{R}_0$ increases through unity and to retain local stability for $\mathscr{R}_0 \leq 1$. An important question to answer, which we shall examine later, is whether this merozoite-free steady state which always exists for all forms of realistic growth rate functions and is locally and asymptotically stable for values of $\mathscr{R}_0 \leq 1$ can have a global stability character for these range of values of $\mathscr{R}_0$. Next, we examine the local stability properties for the parasitized steady state.

Theorem 4 (On the local stability of the parasitized state). *Let $g : [0, \infty) \to \mathbb{R}$ be a real valued function modeling the dynamics of the red blood cell population in the absence of infection as derived above. Let $\mathscr{R}_0 > 1$ be the threshold parameter defined by (3.1). Let r_h^* be the unique nonzero parasitized steady state solution satisfying, for $r_h^* \in (0, 1)$, the equation $g(r_h^*) = A_1 r_h^* - A_0$ where A_1 and A_0 are given by (4.5) with $A_0 \leq A_1 \ \forall \ \mathscr{R}_0 \geq 1$. Then, for each of the type of growth models satisfying Definition 1 as considered here, a realistic steady state solution $r_h^* \in (0, 1)$ satisfying the equation $g(r_h^*) = A_1 r_h^* - A_0$ can exists only if $\frac{A_0}{A_1} < r_h^* < 1$. Moreover, the steady state solution so bracketed, when it exists, its value is uniquely determined and it is locally and asymptotically stable to small perturbations for a range of values of $\mathscr{R}_0 > 1$.*

Proof. The existence of the nonzero steady state solution has been established and summarized in the analysis leading up to the statement of Theorem 1. That the solution exist and lies between the bounds indicated is deduced by noting that the straight line $A_1 r_h^* - A_0$ intercepts the vertical axis at $-A_0$ where $r_h^* = 0$ and intercepts the r_h^* axis at $r_h^* = \frac{A_0}{A_1}$ where $A_1 r_h^* - A_0 = 0$. $\frac{A_0}{A_1} < 1$ whenever $\mathscr{R}_0 > 1$. $g(r_h^*)$ is a unimodal or one hump function that attains a maximum at the point $r_h^* = r_h^m$, where $g'(r_h^m) = 0$ with $g'(r_h^*) < 0$ whenever $r_h^* > r_h^m$, $g'(r_h^*) > 0$ whenever $r_h^* < r_h^m$ and $g(r_h^*) \leq 0$ for all $r_h^* \geq 1$. Thus $g(r_h^*)$ is decreasing from positive values for $r_h^m < r_h^* \leq 1$ and $A_1 r_h^* - A_0$ is increasing from zero for $\frac{A_0}{A_1} \leq r_h^* < r_h^m < 1$. Since both functions are continuous, there exist r_h^* with $r_h^m \leq \frac{A_0}{A_1} < r_h^* < 1$ such that $g(r_h^*) = A_1 r_h^* - A_0$ as illustrated in Fig. 3(c). On the other hand, if $g'(r_h) > 0$ and $\mathscr{R}_0 > 1$, then $r_h < r_h^m < 1$ and $0 < \frac{A_0}{A_1} < r_h^* < r_h^m$; a smaller steady state value as illustrated in Fig. 3(d). When $\mathscr{R}_0 < 1$, the two curves do not intersect for $r_h^* \in [0, 1]$ and a realistic nonzero solution does not exist as illustrated in Fig. 3(a). The solution r_h^* so bracketed is unique because of monotonicity. The local stability of the parasitized steady state solution is then determined by the eigenvalues of the Jacobian matrix at the steady state. We can establish that, for a range of values of $\mathscr{R}_0 > 1$, when the steady state solution is such that $r_h^m < r_h^* < 1$, then $g'(r_h^*) < 0$ and from the coefficients of the characteristic polynomial (4.17), We deduce that $P > 0$, $Q > 0$ and $R > 0$ and $PQ - R > 0$ whenever $\mathscr{R}_0 > 1$, and so there are no zeros of the characteristic polynomial with positive real parts which will signify growing perturbations in the linear regime. However, when the steady state solution is such that $0 < r_h^* < r_h^m < 1$, then for this value of r_h^*, $g'(r_h^*) > 0$ and the sign of $PQ - R$ can change from positive to negative signifying the presence of growing

solutions for those values of $\mathscr{R}_0 > 1$ for which $PQ - R = 0$. Hence the parasitized steady state, when it exists, is locally and asymptotically stable only for a range of values of $\mathscr{R}_0 > 1$. □

The exact character of the stability results so postulated by Theorem 4 will be determined by the nature of the recruitment function used in the analysis. We demonstrate some of these below through more specific results:

Corollary 1. *Let the conditions of Theorem* 4 *continue to apply. Let* $\mathscr{R}_0 > 1$ *and the function* $g : [0, \infty) \to \mathbb{R}$ *be defined by* $g(r_h) = 1 - r_h$. *Let* $\boldsymbol{x}^*$ *be the steady state of system* (2.13)–(2.17) *for which* r_h^* *obtained by solving the equation* $g(r_h^*) = A_1 r_h^* - A_0$, $\mathscr{R}_0 > 1$, *so that the remaining steady state solutions are given by* (4.1)–(4.4). *Then, for all values of* λ, *the eigenvalues of the linearized system defined by the polynomial* (4.17) *evaluated at* $\boldsymbol{x}^*$ *have negative real parts. That is, when* $g(r_h) = 1 - r_h$ *and* $\mathscr{R}_0 > 1$, *then the corresponding steady state is locally and asymptotically stable whenever* $\mathscr{R}_0 > 1$.

Proof. We show that when $g(r_h) = 1 - r_h$, then, at $x = \boldsymbol{x}^*$, $P > 0$, $Q > 0$, $R > 0$ and $PQ - R > 0$ whenever $\mathscr{R}_0 > 1$ and the deduce from the Routh–Hurwitz stability criteria that the computed steady is locally and asymptotically stable. To do this, we need explicit expressions for P, Q and R at these steady states. Now, when $1 - r_h^* = A_1 r_h^* - A_0$, then $r_h^* = \frac{1+A_0}{1+A_1}$, where A_0 and A_1 are given in (4.6). Substituting this value for r_h^* in (4.1)–(4.4) and then in P, Q and R of (4.17), we have

$$P(\boldsymbol{x}^*) = \frac{P_2(\mathscr{R}_0 - 1)^2 + P_1(\mathscr{R}_0 - 1) + P_0}{P_3(\mathscr{R}_0 - 1) + P_4},$$

$$Q(\boldsymbol{x}^*) = \frac{Q_2(\mathscr{R}_0 - 1)^2 + Q_1(\mathscr{R}_0 - 1) + Q_0}{Q_3(\mathscr{R}_0 - 1) + Q_4}, \tag{4.18}$$

$$R(\boldsymbol{x}^*) = \mathscr{R}_0(\mathscr{R}_0 - 1), \tag{4.19}$$

where

$$P_2 = a_0(q_2 + 1)^2(a_2q_1 + a_3 + q_4)^2, \quad \tilde{p}_1 = a_0a_2\beta q_1 + (a_3 + q_4)(q_2 + 1),$$

$$P_1 = \tilde{p}_1(a_2q_1 + a_3 + q_4)(a_0a_2\beta q_1 + (q_2 + 1)(2a_0 + a_3 + q_2 + q_4 + 1)),$$

$$P_0 = (a_2q_1 + a_0 + a_3 + q_2 + q_4 + 1)\tilde{p}_1^2,$$

$$P_3 = (q_2 + 1)(a_2q_1 + a_3 + q_4)\tilde{p}_1, \quad P_4 = \tilde{p}_1^2,$$

$$Q_2 = a_0(q_2 + 1)(a_2q_1 + a_3 + q_4)^2(a_0a_2\beta q_1 + (q_2 + 1)(a_3 + q_2 + q_4 + 1)),$$

$$Q_1 = a_0\tilde{p}_1(a_2q_1 + a_3 + q_4)(a_2\beta q_1(a_0 + q_2 + 1) + 2(q_2 + 1)(a_3 + q_2 + q_4 + 1)),$$

$$Q_0 = a_0(a_2q_1 + a_3 + q_2 + q_4 + 1)\tilde{p}_1^2,$$

$$Q_3 = P_3, \quad Q_4 = P_4, \quad \mathscr{R}_0 = a_0(q_2 + 1)(a_2q_1 + a_3 + q_4).$$

We immediately observe that both $P(\boldsymbol{x}^*) > 0$ and $Q(\boldsymbol{x}^*) > 0$ are larger than $R(\boldsymbol{x}^*) \geq 0$ independently whenever $\mathscr{R}_0 \geq 1$. So $P(\boldsymbol{x}^*)Q(\boldsymbol{x}^*) - R(\boldsymbol{x}^*) > 0$. Therefore, the Routh–Hurwitz stability criteria assure us that the computed steady state is locally and asymptotically stable to small perturbations whenever $\mathscr{R}_0 > 1$. □

The result of Corollary 1 assures us that when the recruitment function is linear as prescribed, the parasitized steady state is locally asymptotically stable, for all values of $\mathscr{R}_0 > 1$. However, the next result shows that when the recruitment function is sufficiently nonlinear, then the parasitized state is stable for a range of values of $\mathscr{R}_0 > 1$ but also can be driven to instability via a Hopf bifurcation for sufficiently large values of $\mathscr{R}_0$.

Corollary 2. *Let the conditions of Theorem* 4 *continue to apply. Let* $\mathscr{R}_0 > 1$ *and the function* $g : [0, \infty) \to \mathbb{R}$ *be defined by* $g(r_h) = r_h(1 - r_h)$. *Let* $\boldsymbol{x}^*$ *be the positive steady state of system* (2.13)–(2.17) *for which* r_h^* *is obtained by solving the equation* $g(r_h^*) = A_1 r_h^* - A_0$, $\mathscr{R}_0 > 1$, *so that the remaining steady state solutions are given by* (4.1)–(4.4). *Then, all values of* λ, *the eigenvalues of the linearized system defined by the polynomial* (4.17) *evaluated at* $\boldsymbol{x}^*$ *have negative real parts for* $1 < \mathscr{R}_0 < \mathscr{R}_0^c$, *and at* $\mathscr{R}_0 = \mathscr{R}_0^h$ *the steady state loses stability to periodic solutions with fixed amplitude and period. That is, when* $g(r_h) = r_h(1 - r_h)$ *and* $\mathscr{R}_0 > 1$, *then the corresponding steady state is locally and asymptotically stable only for a range of values of* $\mathscr{R}_0 > 1$.

Proof. The stability of the steady state is determined by the sign of the eigenvalues given by the solutions of the polynomial (4.17). We show that there exist a value of $\mathscr{R}_0^c > 1$ such that $PQ = R$ at which point λ, a solution on (4.17) is purely imaginary, and that as $\mathscr{R}_0$ increases further from $\mathscr{R}_0^c > 1$, λ, a root of (4.17) has a positive real part. For this we consider the function $P(\mathscr{R}_0)Q(\mathscr{R}_0) - R(\mathscr{R}_0)$ at the steady state $\boldsymbol{x}^*$, where $r_h^*(\mathscr{R}_0)$ is given by (4.7), and note that at $\mathscr{R}_0 = 1$, $\boldsymbol{x}^* = (1, 0, 0, 0, 0)$ and that by Lemma 1, we have that $r_h^* \to 0$ as $\mathscr{R}_0 \to \infty$. We thus have that, on the one hand, as $\mathscr{R}_0 \to 1^+$, $P(\mathscr{R}_0)Q(\mathscr{R}_0) - R(\mathscr{R}_0) \to a_0(a_2q_1 + a_3 + q_2 + q_4 + 1)(a_2q_1 + a_0 + a_3 + q_2 + q_4 + 1) > 0$ while as $\mathscr{R}_0 \to \infty$, $P(\mathscr{R}_0)Q(\mathscr{R}_0) - R(\mathscr{R}_0) \to (a_0 - q_2 - 1)(a_3 + q_2 + q_4 + 1) < 0$ whenever either $1 + q_2 < a_0 < a_3 + q_4$ or $a_3 + q_4 < a_0 < 1 + q_2$. Only one of these inequalities is possible whenever the target limit is negative. Thus, from the continuity of $P(\mathscr{R}_0)Q(\mathscr{R}_0) - R(\mathscr{R}_0)$ as a function of $\mathscr{R}_0 \in [1, \infty)$, there exist $\mathscr{R}_0^c \in (1, \infty)$ such that $P(\mathscr{R}_0^c)Q(\mathscr{R}_0^c) - R(\mathscr{R}_0^c) = 0$. At this point, the polynomial (4.17) then satisfies the equation $\lambda^3 + P\lambda^2 + Q\lambda + PQ = 0$ so $\lambda(\mathscr{R}_0^c) = P$ or $\lambda(\mathscr{R}_0^c) = \pm i\sqrt{Q}$. When $\mathscr{R}_0$ further increases from $\mathscr{R}_0^c$, one of the solutions for λ now has a positive real part and we have growing oscillatory solutions in the linear regime. To determine the initial amplitude and phase of the oscillations as $\mathscr{R}_0$ increases further through $\mathscr{R}_0^c$, we introduce the parameter $\xi = \frac{R}{PQ}$ so that $R = \xi PQ$ and for $\mathscr{R}_0 < \mathscr{R}_0^c$, $\xi < 1$, at $\mathscr{R}_0 = \mathscr{R}_0^c$, $\xi = 1$ and for $\mathscr{R}_0 > \mathscr{R}_0^c$, $\xi > 1$, and view an increase in $\mathscr{R}_0$ as an increase in ξ so that at $\xi = \xi_c = 1$, we have $\mathscr{R}_0 = \mathscr{R}_0^c$. Set $\xi = \xi_c + \varepsilon^2\nu$, where $\nu = \pm 1$. We have here a perturbation near the

point $\xi = \xi_c$ where $\varepsilon \ll 1$, but otherwise arbitrary. Then by Taylor's expansion we have $\lambda(\xi_c + \varepsilon^2\nu) = \lambda(\xi_c) + \lambda'(\xi_c)\varepsilon^2\nu + O(\varepsilon^4)$, so that neglecting the terms of order ε^4 in the calculation, we have the approximation

$$\lambda'(\xi_c) \approx \frac{P(\mathscr{R}_0^c)(Q(\mathscr{R}_0^c) \pm P(\mathscr{R}_0^c)\sqrt{Q(\mathscr{R}_0^c)}i)}{2(Q(\mathscr{R}_0^c) + P(\mathscr{R}_0^c)^2)}.$$

Thus after the perturbation,

$$\lambda(\xi_c + \varepsilon^2\nu) = \pm i\sqrt{Q(\mathscr{R}_0^c)} + \left(\frac{P(\mathscr{R}_0^c)(Q(\mathscr{R}_0^c) \pm P(\mathscr{R}_0^c)\sqrt{Q(\mathscr{R}_0^c)}i)}{2(Q(\mathscr{R}_0^c) + P(\mathscr{R}_0^c)^2)}\right)\varepsilon^2\nu + O(\varepsilon^4). \quad (4.20)$$

Thus the initial period and amplitude of the oscillations are

$$\text{Amplitude} = \exp\left(\frac{PQ}{2(P^2+Q)}\varepsilon^2\nu t\right), \quad \text{Period} = \frac{2\pi}{\sqrt{Q} + \frac{P^2\sqrt{Q}}{2(P^2+Q)}\varepsilon^2\nu}, \quad (4.21)$$

where $\varepsilon \ll 1$ but otherwise arbitrary. □

Observe that if $\nu > 0$ then, we have growing perturbations in the linear regime which we expect that these growing perturbations will be bounded by nonlinearities in the nonlinear regime leading to limit cycles with small amplitude. We emphasize that the perturbations will be small because at this stage the steady state values are very small. A result similar to that of Corollary 2 can be stated and proved for any of the more nonlinear growth rate function with the desired properties as postulated by Definition 1. Though the procedures become more intricate as the nonlinearity in the function g is increased. We shall later illustrate some of these results graphically via numerical simulations.

The results of Theorems 2–4 are local and do not apply to the whole nonlinear system. We next demonstrate that with an appropriate restriction of the parameter values of the system, we can discuss a global stability property for the system at the level of the parasite free steady state solution. We start by noting that Theorem 3 assures us that whenever $\mathscr{R}_0 < 1$, the parasite free steady state which always exists, is locally and asymptotically stable to small perturbations. When $\mathscr{R}_0 = 1$, we have a zero eigenvalue in the linear regime and then we cannot pronounce, with certainty, on the stability property of the parasite-free steady state solution. The next results shows that we can indeed achieve global stability of the parasite-free state provided we maintain $\mathscr{R}_0 \leq 1$. A global stability result of this nature is important as it shows that with appropriate intervention and conditioning of the biological system, we can achieve global results for the entire system so that the parasite-free state is always attainable by controlling the properties of the system, such as by ensuring that $\mathscr{R}_0 \leq 1$.

Theorem 5 (On the Global stability of the merozoite-free steady state). *Let the real valued function $g : [0,\infty) \to \mathbb{R}$ be a recruitment function satisfying the required conditions. Then the merozoite-free equilibrium solution define by $E_{r_h^* \neq 0} = (r_h^*, 0, 0, 0, 0)$, which always exist for all parameter values, is locally and asymptotically stable whenever $\mathscr{R}_0 \leq 1$. Moreover, the particular merozoite-free (parasite-free) steady state solution where $r_h^* = 1$ which can be constructed for all forms of the recruitment function is globally and asymptomatically stable whenever $\mathscr{R}_0 \leq 1$.*

Proof. We start by observing that in the absence of infection, the scaled equation for the red blood cell population satisfies the equation $\frac{dr_h}{dt} = a_0 g(r_h)$ where $g : [0,\infty) \to \mathbb{R}$ is a unimodal or one hump function which attains a maximum at some point $r_h^m \in [0,1]$. Thus $g(r_h) + \mu_h r_h$ also attains a maximum at some point $\tilde{r}_h^m \in [0,1]$ whenever $0 \leq \mu < 1$. Let $a_0(g(\tilde{r}_h^m) + \mu \tilde{r}_h^m) = \tilde{g}^m$. Then, we can construct the inequality $\frac{dr_h}{dt} + a_0 \mu r_h \leq \tilde{g}^m$. Thus integrating this via integrating factor method we have $r_h(t) \leq r_h(0) e^{-a_0 \mu t} + \frac{\tilde{g}^m}{a_0 \mu}(1 - e^{-a_0 \mu t})$. Thus $\lim_{t\to\infty}(\sup_t r_h(t)) < \infty$ and $r_h(t)$ is bounded as expected. In fact, we expect $0 < r_h(t) \leq 1$ when we stay within the limitations of the scaling done in this paper. Thus for any $\epsilon > 0$, we define the closed set

$$\begin{aligned}\mathscr{D} = \{(r_h, r_p, m, g_e, g_l) \in \mathbb{R}^5 : \varepsilon \leq r_h \leq 1, 0 \leq r_p \leq r_p^\infty,\\ 0 \leq m \leq m^\infty, 0 \leq g_e \leq g_e^\infty, 0 \leq g_l \leq g_l^\infty\},\end{aligned}$$

where $0 < \varepsilon \ll 1$ and $r_p^\infty, m^\infty, g_e^\infty, g_l^\infty$ are the respective standardized upper bounds of the associated variables obtainable from the upper bounds $R_p^\infty, M^\infty, G_e^\infty, G_l^\infty$, and the function $V : \mathscr{D} \to \mathbb{R}$ by

$$V(r_h, r_p, m, g_e, g_l) = \tilde{b}_0(r_h - 1 - \ln(r_h) + \tilde{b}_1 r_p + \tilde{b}_2 m + \tilde{b}_3 g_e + \tilde{b}_4 g_l,$$

where

$$\tilde{b}_0 = \frac{(\tilde{b}_2 - 1)(a_3 + q_4)}{a_1 q_1}, \quad \tilde{b}_1 = \frac{(a_2 q_1 + a_3 + q_4)((\tilde{b}_2 - 1) + \mathscr{R}_0)}{a_1 q_1},$$

$$\tilde{b}_3 = \frac{(\tilde{b}_2 - 1)(q_2 + 1)(a_2 q_1 + a_3 + q_4)(1 - \mathscr{R}_0)}{a_1 a_4 q_1 q_3 \sigma},$$

$$\tilde{b}_4 = \frac{(\tilde{b}_2 - 1)(q_2 + 1)(a_2 q_1 + a_3 + q_4)(a_4 + q_5)(1 - \mathscr{R}_0)}{a_1 a_4 a_5 q_1 q_3 q_6 \sigma}.$$

Clearly when $\mathscr{R}_0 \leq 1$ and $\tilde{b}_2 > 1$, then $\tilde{b}_i, i = 0, 1, 2, 3, 4$ are all non-negative. Furthermore $V(r_h, r_p, m, g_e, g_l) > 0$ for all $(r_h, r_p, m, g_e, g_l) \in \mathscr{D} \backslash \{(1, 0, 0, 0, 0)\}$ and $V(1, 0, 0, 0, 0) = 0$. Thus V is positive definite and can serve as a Lyapunov

function. Along the solution trajectories of the system, we have

$$\begin{aligned}\frac{dV}{dt} &= \nabla V \cdot \left(\frac{dr_h}{dt}, \frac{dr_p}{dt}, \frac{dm}{dt}, \frac{dg_e}{dt}, \frac{dg_l}{dt}\right)\\ &= \tilde{b}_0\left(1-\frac{1}{r_h}\right)(a_0 g(r_h) - a_1 q_1 m r_h) + \tilde{b}_1(a_1 q_1 m r_h - (1+q_2)r_p)\\ &\quad + \tilde{b}_2(a_2[q_3(1-\sigma)r_p - q_1(r_h+\beta r_p)m] - (a_3+q_4)m)\\ &\quad + \tilde{b}_3(a_4[q_3\sigma r_p - g_e] - q_5 g_e) + \tilde{b}_4(a_5[q_6 g_e - g_l] - q_7 g_l)\\ &= \tilde{b}_0\left(1-\frac{1}{r_h}\right)a_0 g(r_h) - (a_3+q_4)m - \tilde{b}_2 a_2 q_1 \beta r_p m - \tilde{b}_4(a_5+q_7)g_l\\ &\quad + ((a_2 q_1 + a_3 + q_4)\mathscr{R}_0 - a_2 q_1)m r_h.\end{aligned}$$

Given that $0 \le r_h \le 1$, we deduce that $0 \ge -(a_3+q_4)mr_h \ge -(a_3+q_4)m$ leading to

$$\begin{aligned}\frac{dV}{dt} &\le \tilde{b}_0\left(1-\frac{1}{r_h}\right)a_0 g(r_h) - \tilde{b}_2 a_2 q_1 \beta r_p m\\ &\quad - \tilde{b}_4(a_5+q_7)g_l - (a_2 q_1 + a_3 + q_4)(1-\mathscr{R}_0)m r_h.\end{aligned}$$

We then note that $\left(1-\frac{1}{r_h}\right)g(r_h) \le 0$ whenever $0 < r_h \le 1$ since

$$\left(1-\frac{1}{r_h}\right)g(r_h) = \begin{cases} -\dfrac{(1-r_h)^2}{r_h} & \text{if } g(r_h) = 1-r_h,\\ -(1-r_h)^2 & \text{if } g(r_h) = r_h(1-r_h),\\ -(1-r_h)(e^{\ln(\mu)r_h} - \mu) & \text{if } g(r_h) = r_h(e^{\ln(\mu)r_h} - \mu),\\ -(1-r_h)\left(\dfrac{1}{1+\left(\frac{1}{\mu}-1\right)r_h^n} - \mu\right) & \text{if } g(r_h) = r_h\left(\dfrac{1}{1+\left(\frac{1}{\mu}-1\right)r_h^n} - \mu\right).\end{cases}$$

It is then evident that $V'(t) \le 0$ whenever $\mathscr{R}_0 \le 1$. In all we have the following: (i) $V' < 0$ if $\mathscr{R}_0 \le 1$, for all t and $\forall \boldsymbol{x} \in \mathscr{D} \setminus \{(1,0,0,0,0)\}$; (ii) $V(\boldsymbol{x}) = 0$ at $\boldsymbol{x} = \boldsymbol{x}_f$ and (iii) $V(\boldsymbol{x}) > 0, \forall \boldsymbol{x} \in \mathscr{D}$ with $\boldsymbol{x} \ne \boldsymbol{x}_f$. Thus, V is a positive definite function and $\{\boldsymbol{x}_f\}$ is the largest invariant compact subset in $\{(0,1]\times\mathbb{R}^4_+ | V'(t) = 0\}$ containing only the equilibrium $\boldsymbol{x}_f$ when $\mathscr{R}_0 \le 1$, then by LaSalle's invariance principle, the parasite-free steady state solution $\boldsymbol{x}_f = (1,0,0,0,0)$ of system (2.23)–(2.27) is globally asymptotically stable whenever $\mathscr{R}_0 \le 1$. □

5. Illustrations and Numerical Simulations

In this section, we illustrate the linear analysis presented through a numerical example. We then run some numerical simulations to showcase the richness of the results

studied in this paper. The baseline parameters used in the example are as explained in Ref. 22 (also see Supplementary Section B). We do not return to the original parameters of the system here, but rather use only the scaled parameter values to illustrate our work. A more biological interpretation based on the original parameters of the model shall be presented elsewhere. We use the fact that an increase in the scaled parameter value a_1 will lead to an increase in $\mathscr{R}_0$ throughout this section. We use the following base example.

Example 1 (An illustrative example parameter set). Consider the baseline parameters, whose provenance and form has been explained in Ref. 29, and with possible ranges shown in Supplemental Document B.

$$\begin{aligned}
&a_2 = 50, \quad a_3 = 95, \quad a_4 = \frac{85}{100}, \quad a_5 = \frac{6}{10}, \quad a_0 = \frac{5}{10},\\
&\rho_1 = \frac{613}{10^4}, \quad \rho_2 = 585 \times 10^2, \quad \rho_3 = \frac{57}{10^3},\\
&\rho_4 = 676 \times 10^2, \quad \rho_5 = \frac{613}{10^4}, \quad \rho_6 = 235 \times 10^2, \quad \rho_7 = \frac{33}{10^5}\\
&p_0 = \frac{17}{100}, \quad p_1 = \frac{24}{100}, \quad p_2 = \frac{12}{100}, \quad \beta = \frac{75}{100}, \quad \sigma = \frac{6}{1000},\\
&e_i = \frac{9}{10}, \quad e_a = 5 \times 10^{-5}, \quad q_1 \approx 0.999, \quad q_2 \approx 1.48,\\
&q_3 \approx 0.9998, \quad q_4 \approx 1.59, \quad q_5 \approx 0.625, \quad q_6 \approx 0.9999, \quad q_7 \approx 0.0003.
\end{aligned} \tag{5.1}$$

Here, the innate immune response is operating at 90% performance (contextually, it is operating at 90% of its maximal steady state size in the absence of infection), but the adaptive immunity is operational but very small. Extreme values for different snapshots of the immunity-based variables were used with similar qualitative results.

5.1. *Illustration: Boundedness of the parasitized steady state solution*

Lemma 1 assures us that the size of the steady state red blood cell population r_h^* decreases to zero as $\mathscr{R}_0$ increases from unity. We understand this phenomenon by noting that as the infection and systematic parasitization and destruction of healthy red blood cells starts, we expect that the scaled red blood cell population density will start dropping while the density of the parasitized and free merozoite populations will increase. However, as more and more red blood cells get destroyed, the density of parasitized red blood cells will then start dropping as $\mathscr{R}_0$ further increases from unity. Using the expressions for the steady state values as well as the parameters shown in Example 1, we numerically computed the steady states for different values of the parameter a_1. As shown in Fig. 4, the nonzero steady states

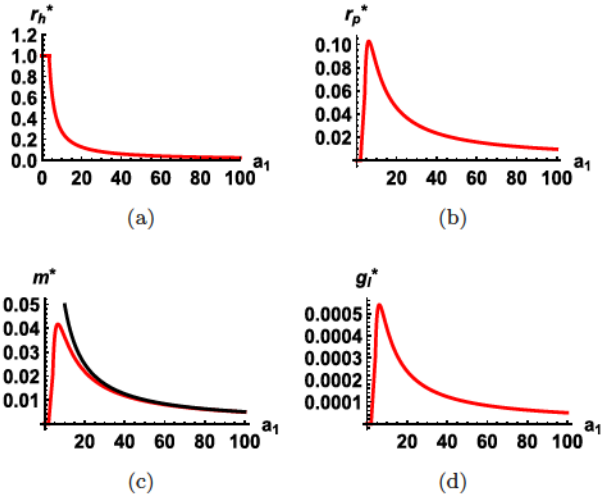

Fig. 4. Figure showing the size of the steady states as $\mathscr{R}_0$ increases when all other parameters are fixed as in Example 1. Here, a_1 increases from 0 to 100, which corresponds to $\mathscr{R}_0$ increasing from 0 to 35. We see clearly that as $\mathscr{R}_0$ increases from zero, the size of r_h^*, the scaled red blood cell steady state density when $g(r_h) = r_h(1 - r_h)$ continues to drop as predicted by Lemma 1. However, in the initial phase of the infection process, the size of the steady state for the parasitized red blood cells and merozoite populations initially increase with increasing $\mathscr{R}_0$ before dropping as less and less red blood cells are available for parasitization. Graph (c) shows that the merozoite steady state population is always bounded above by $\frac{a_0}{a_1}$ as reported in Ref. 29.

which exist only for values of $\mathscr{R}_0 > 1$ (corresponding to $a_1 \geq 7.3$ for this particular set of parameter values), are all bounded and approach zero for large values of $\mathscr{R}_0$.

We note that the size of the parasitized steady state approaches zero asymptotically but is never zero. This small state is, at all times, different from the zero state which only exists when there are no red blood cells in the system. It is caused by severe destruction of red blood cells because of the action of the parasite. In agreement with the results reported in Ref. 29, the merozoite density always satisfies the inequality $m^* < \frac{a_0}{a_1}$ and so approach small values as a_1 increases for fixed a_0. The parameter a_0 is linked with the linear rate of recruitment of healthy red blood cells while a_1 is linked to the number of merozoite released by each bursting red blood cell. It is therefore clear that when parasitization is severe, a_1 will also get large when the regulated linear rate of production of healthy red blood cells will be approximately constant.

5.2. *Illustration: Occurrence of the hopf bifurcation*

To numerically ascertain the stability of the steady state solution as $\mathscr{R}_0$ increases from unity as well as verify the results of Corollary 2, we numerically computed the eigenvalues of the linearized system as established by the polynomial (4.16) for different values of $\mathscr{R}_0$. Figure 5 shows a plot of the size of the maximum of the

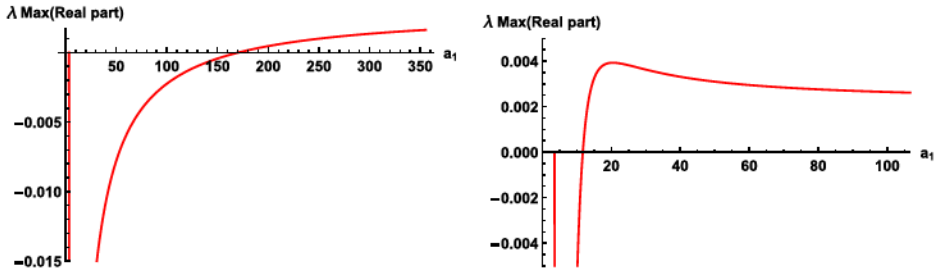

(a) (b)

Fig. 5. Figure showing the sign of the maximum real part of the eigenvalues λ computed by solving equation (4.16) based on Example 1 parameters and for different values of $\mathscr{R}_0$. $\mathscr{R}_0$ was increased by varying a_1 when all other parameters of the system and the recruitment function are fixed. For the graph on the left, $g(r_h) = r_h(1 - r_h)$ and a_1 increases from 0 to over 350, which corresponds to $\mathscr{R}_0$ increasing from 0 to 100. The maximum eigenvalue becomes positive at $a_1 \approx 170$, corresponding to the value $\mathscr{R}_0 \approx 47.8$. For the graph on the right, $g(r_h)$ is the Maynard–Smith–Slatkin growth function and a_1 increases from 0 to over 100, which corresponds to $\mathscr{R}_0$ increasing from 0 to 30. The maximum eigenvalue becomes positive at $a_1 \approx 12$, corresponding to the value $\mathscr{R}_0 \approx 3.38$. We see clearly in each case that as $\mathscr{R}_0$ increases further away from unity, the maximum real part of the eigenvalues is increasing from negative values and becomes zero at that point which corresponds to a critical value of $\mathscr{R}_0 = \mathscr{R}_0^c$ as predicted by Corollary 2.

real parts of the eigenvalues of the linearized system. Clearly, as $\mathscr{R}_0$ increases from unity, the maximum real part of the eigenvalues is negative signifying stability of the parasitized steady state. As $\mathscr{R}_0$ further increases from unity, as predicted by Corollary 2, a point is reached where the maximum real part of the eigenvalues changes from positive to negative signifying the onset of exponentially growing solutions with a growing solutions in the linear regime. We noted, as shown in Fig. 5 that the different recruitment functions offer different quantitative results, though the qualitative results are the same. For example, for the logistic growth model, we require larger values of $\mathscr{R}_0$ for the system to lose stability, to oscillatory solutions than for the Maynard–Smith–Slatkin growth model, while as established here and earlier reported in Ref. 29, the linear growth model does not admit a parameter regime whereby the parasitized state loses stability for any value of $\mathscr{R}_0$.

5.3. *Illustration: The different solution types*

For $\mathscr{R}_0$ values in ranges for which the maximum real part of the eigenvalues of the linearized system is negative, we expect the system to converge to the parasitized steady state long term, as shown in Figs. 6 and 7. As $\mathscr{R}_0$ further increases there is a point in the parameter space, as postulated by Corollary 2, where the maximum real part changes from negative to positive signifying the emergence of growing oscillatory solutions, and we expect that the growing oscillations will be bounded by nonlinearity and we can observe limit cycle or fixed amplitude oscillating solutions as shown in Figs. 9 and 8. The limit cycle solution for these plots are shown in Figs. 10 and 11, illustrating phase plane plots for r_h versus r_p and r_h versus m.

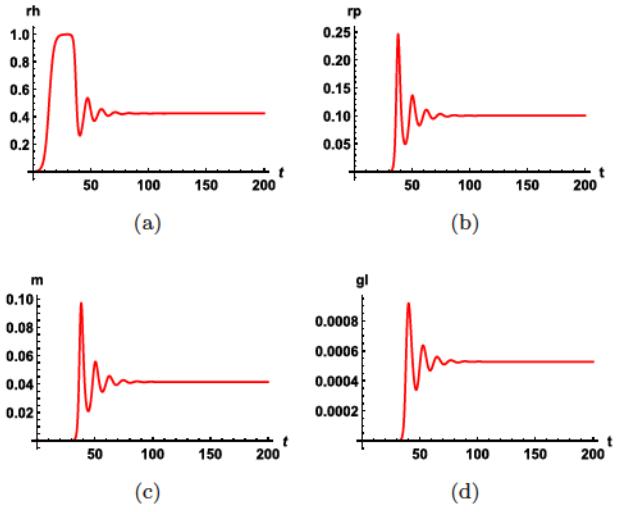

Fig. 6. Long-term solution dynamics for values of $\mathscr{R}_0$ in the range where we have stable endemic non-periodic solutions with fixed amplitude. $\mathscr{R}_0 = 1.95$. The rest of the parameters are as in Example 1 and $g(r_h)$ is the logistic growth function.

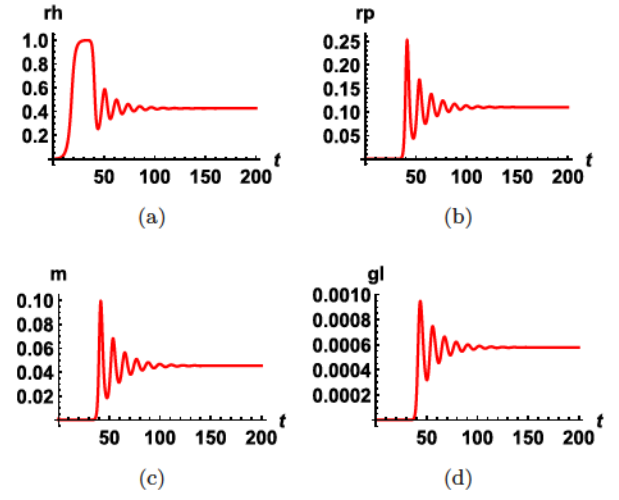

Fig. 7. Long-term solution dynamics for values of $\mathscr{R}_0$ in the range where we have stable endemic non-periodic solutions with fixed amplitude. $\mathscr{R}_0 = 1.95$. The rest of the parameters are as given in Example 1 and $g(r_h)$ is the Maynard–Smith–Slatkin recruitment function with $\mu = \frac{3}{10}$, $n = 4$.

The behavior that we are seeing is consistent with the assumptions of the model derived. We believe that the oscillations we are seeing for large values of $\mathscr{R}_0$ to be indicative of the system compensating through massive cell death and reparasitization. The nature of the oscillations depend on the type of recruitment function used and is indicative of richness of the model studied in this paper. In the absence

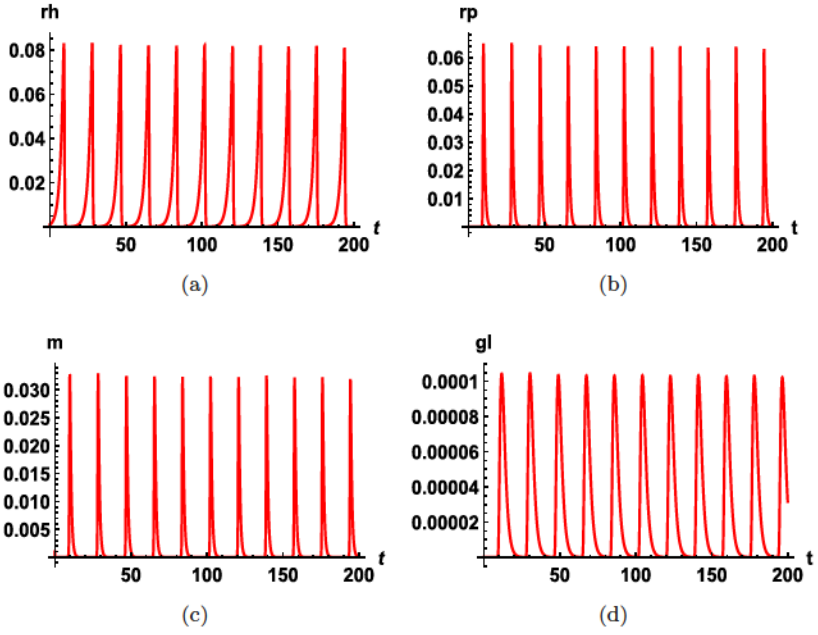

Fig. 8. Long-term solution dynamics for $\mathscr{R}_0 = 58.23$ using Example 1 parameters, with $g(r_h)$ the logistic recruitment function. Only ranges where there are periodic solutions with fixed amplitude are shown. All plots start at $(0, 0)$.

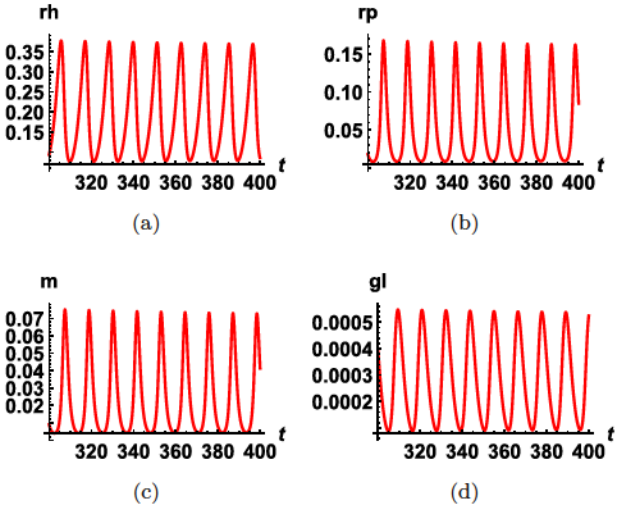

Fig. 9. Long-term solution dynamics for $\mathscr{R}_0 = 3.95$ using Example 1 parameters, with $g(r_h)$ the Maynard–Smith–Slatkin recruitment function where $\mu = \frac{3}{10}$, $n = 4$. Only ranges where there are periodic solutions with fixed amplitude are shown. For all four plots, t starts at 300, while r_h, r_p, m and g_l start at 0.085, 0, 0.004 and 0.00008, respectively.

of real data to describe the true nature of the recruitment functions as modeled via a single function, we can only say that the restriction of previous studies to using the linear or constant recruitment term has hitherto hidden the richness of results possible for the within-human host dynamics of the *P. falciparum* parasite.

We remark, here, that the total red blood cell density in a malaria patient exhibiting the dynamics as illustrated in Figs. 6–11 can be computed by either summing the steady state densities for r_h and r_p, or the corresponding maximal and minimal bounds, in the scenarios where there are limit cycles. From Figs. 6, 7(a) and 7(b), the sum, which is given in nondimensional form, is about 0.55 when using the logistic growth model, which is similar in size to the value when using the Maynard–Smith–Slakin recruitment function for the specified parameters. In the original variables, we can compute these values by using the scaled variables described in Eqs. (2.10) and (2.11). That is, $R_h = r_h R_h^0$ and $R_p = r_p R_p^0$ where we had chosen in Eq. (2.11), $R_h^0 = R_p^0 = \frac{\lambda_h - \mu_h}{\tilde{\mu}_h}$ for the logistic model and $R_h^0 = R_p^0 = K_h\left(\frac{1}{\mu} - 1\right)^{\frac{1}{n}}$ for the Maynard–Smith model. K_h, is the maximal red blood cell

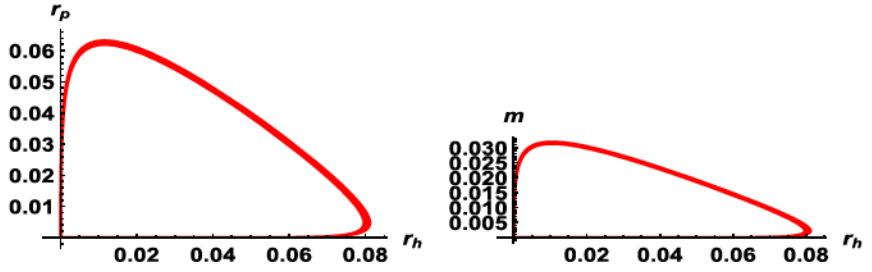

(a) (b)

Fig. 10. Figure showing the existence of the limit cycle for the logistic recruitment function. $\mathscr{R}_0 = 58.23$. The rest of the parameters are as given Example 1 and $g(r_h)$ is the logistic growth model.

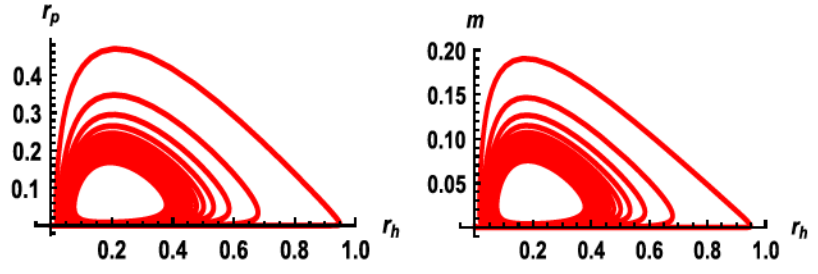

(a) (b)

Fig. 11. Figure showing the existence of the limit cycle for the Maynard–Smith–Slatkin recruitment function with $\mu = \frac{3}{10}$, $n = 4$. $\mathscr{R}_0 = 3.95$. The rest of the parameters are as given Example 1 and $g(r_h)$ is the Maynard–Smith–Slatkin recruitment function with $\mu = \frac{3}{10}$, $n = 4$.

count, which serves as the carrying capacity for the Maynard–Smith model. This value lies in the range 10^6–10^7 cells per μL, meanwhile, the equivalent term for the logistic model is $K = \frac{\lambda_h - \mu_h}{\tilde{\mu}_h}$ where in Ref. 22, we obtained an estimate for $\tilde{\mu}_h$ to be in the range 3.6×10^{-9}–5.0×10^{-7}. Holding all parameters fixed and for the choices of μ and n as illustrated in Figs. 7, 9 and 11, we can choose feasible values for λ_h, β_1 (hence β_2 and β_3) and the other parameters, with K_h and $\tilde{\mu}_h$ in the given ranges such that $a_0 > 0$, $a_2 > 0$, $a_3 > 1$ and $0 < a_4, a_5 < a_3$ and the example parameters in (5.1) are satisfied. We begin computing these estimates for the examples for which $\mathscr{R}_0 = 1.95$, that is Figs. 6 and 7. First, from Fig. 6, the logistic case, and the nondimensional expression for a_2, we can estimate that when $r_h + r_p = 0.6$, corresponding estimates for R_h lies in the range 1.53×10^6 and higher depending on choices of other parameters. This is within observable ranges in various studies (see for example observed red blood cell densities in a study on patients diagnosed with malaria in Thailand[58] and also the study in Ref. 59). Similar calculations can be carried out for the Maynard–Smith example. Thus, our scaled values correspond to non-scaled values that have been observed in nature. However, the small values associated to $r_h + r_p$ are for heavily parasitized patients, which can be used as a proxy to indicate the degree of anemia in these patients.

6. Discussion and Conclusion

6.1. *Discussion*

Our goal in this paper was to understand the implicit role immunity plays in the within-human-host dynamics of the *P. falciparum* parasite for different recruitment functions for the HRBCs. The model studied was originally developed in Refs. 22 and 29 in its entirety, but was only analyzed under the assumption of immunity suppression and for two types of healthy red blood cells recruitment functions — linear and logistic. The model developed took into consideration the human adaptive immune response developed due to continuous exposure to the malaria disease as well as the innate adaptive immune responses, the body's natural fighting mechanism against foreign pathogens. It captured the interaction between the two types of immune cells, innate and adaptive, implicitly illustrating their role in inhibiting the processes leading to a successful parasite persistence within a human infected with the malaria parasite, as well as their individual impacts. The results under immunity suppression indicated that a more nonlinear recruitment function should be used to model HRBCs recruitment, as the linear model produced an increasing merozoite size, regardless of the diminishing effect of the HRBC population. Thus the logistic function was a better choice model over a linear function for modeling HRBC recruitment.

Here, we have extended the work in Ref. 29, incorporating other types of recruitment functions, specifically the Ricker and Maynard–Smith–Slatkin recruitment functions. We then used these functions to investigate the role of immunity on

the malaria dynamics process, especially the role of the acquired (adaptive) immunity. In our model, our general assumption was that the net effect of the action of the immune system is to slow down, if not arrest, the process of invasion by the malaria parasite. The "slowing down effects" via inhibition of parasitemia, formation of gametocytes, key biological feasible processes mentioned in the literature, were captured through the scaled functions of e_a and/or e_i through the expressions $\frac{1}{1+p_k e_a}$ and $-\rho_i(1+\rho_{i+1}e_a)e_i$, $k=0,1,2$ and $i=1,\ldots,7$ in the model, which allowed us to view the scale variables e_a and e_i, simply as parameters with sizes, respectively, in the intervals $[0,\infty)$ and $[0,1]$.

Our model results indicate that the parasitemia threshold function, $\mathscr{R}_0$, the function that determines whether the parasite succeeds to invade the human's HRBCs and eventually render the human infectious to mosquito, was much smaller than the threshold for the model in which the adaptive immune response was set to zero, and this threshold was even much smaller for the case under complete immunity suppression obtained in Ref. 29. That is, we had

$$\mathscr{R}_0 = \underbrace{\frac{a_1 a_2 q_1 q_3(1-\sigma)}{(q_2+1)(a_2 q_1+a_3+q_4)}}_{\text{active } e_a>0 \text{ and } e_i\in(0,1)} \leq \underbrace{\frac{a_1 a_2(1-\sigma)}{(1+\rho_1)(a_2+a_3+\rho_3)}}_{e_a=0,e_i=1} \leq \underbrace{\frac{a_1 a_2(1-\sigma)}{(a_2+a_3)}}_{e_a=0,e_i=0}.$$

This inequality illustrates the following: (i) expresses the fact that $\mathscr{R}_0$ will increase with decreasing effectiveness of the adaptive immune response and both immune responses, (ii) indicates that $\mathscr{R}_0$ attains its maximum value when both the innate and adaptive immune responses are zero (iii) captures the expectation that as adaptive immunity kicks into action following repeated parasitemia, the value and size of the parasitemia reproduction number will continue to reduce in size. We believe that the above three results are important for malaria parasitemia control as results (i) and (ii) assure us that even in the absence of the immune response, the parasitemia reproduction number can be bounded; even though $\mathscr{R}_0$ can continue to increase with increasing a_1. Result (iii) indicates that the value of $\mathscr{R}_0$ and hence the strength of parasitization of the red blood cells is reduced when the combined effect of these immunity-based responses are operating at maximal levels. The parameterized parameter $\mathscr{R}_0$ so identified can thus be used to study the behavior of the system in the presence of immunity. This is evident as shown in Fig. 4, where if we view a reduction in $\mathscr{R}_0$ as a reduction in the size of the immunity parameters, an $\mathscr{R}_0$ value close to 1 but bigger than 1 (strong immunity effects on parasitemia), shows that the steady state size of the HRBCs is closer to 1, its maximal value, compared to when $\mathscr{R}_0$ is large (weak immunity effects on parasitemia) showing that the steady state size of the HRBCs reduces, approaching zero for increasingly larger $\mathscr{R}_0$.

Another question of interest is how the choice of the recruitment or growth function that models HRBC population in the absence of infection, impacts the overall model dynamics. Four types of growth functions were considered: linear, logistic,

Ricker and the Maynard–Smith–Slatkin growth functions. We showed that the trivial steady state, which only existed for the more nonlinear recruitment functions — logistic, Ricker and Maynard–Smith–Slatkin functions, is always unstable. On the other hand, the parasite-free steady state, the desirable steady state, which exists for all four types of growth functions is globally asymptotically stable when the parasitemia reproduction number $\mathscr{R}_0$ is less than unity. Additionally, a unique parasitized steady state exists for all four types of recruitment functions. The behavior of the parasitized steady state depends on whether the HRBC recruitment function is linear or nonlinear. For the linear case as is prescribed in Sec. 2.2, we showed that the parasitized steady state is locally asymptotically stable, for all values of $\mathscr{R}_0 > 1$, with the size of r_h diminishing down toward zero with increasing $\mathscr{R}_0$ values, meanwhile the size of the merozoite population grows to a large value. On the other hand, for a sufficiently nonlinear recruitment function such as the logistic, Ricker, and Maynard–Smith–Slatkin functions, the parasitized state is stable for a range of values of $\mathscr{R}_0 > 1$ but also can be driven to instability via a Hopf bifurcation for sufficiently large values of $\mathscr{R}_0 > 1$, leading to a limit cycle as shown in Figs. 8–11. The instability, leading to limit cycles does not occur for the linear model.

In particular, as a function of the steady state HRBC population, r_h^*, the merozoite steady state size, m^*, attains a maximum at some point given by Eq. (4.12). The increase in the size of the steady state merozoite population up to its maximum is associated with a decrease in the size of the steady state HRBC population. However, as the parasite threshold parameter $\mathscr{R}_0$ increases further, which could be as a result of higher contacts, inefficient immune response, etc. more and more HRBCs are parasitized. As more and more HRBCs are parasitized, the steady state size of the HRBC population continues to decrease. For the nonlinear growth functions, there comes a time when the steady state parasite populations, merozoites and parasitized red blood cells, start to decline as there is not a large pool of HRBCs to infect. We conjecture that eventually, the recruitment rate of the HRBCs balances out their destruction effect through parasitemia, leading to sustained bounded oscillations of the steady states of HRBC populations, as well as the merozoite, IRBC and gametocyte steady state populations. Hence the observed limit cycle. We note that the limit cycles for a more nonlinear function, like the Maynard–Smith–Slatkin birth rate function commences at an $\mathscr{R}_0$ threshold value that is not quite large (shown for $\mathscr{R}_0 = 4.15$ but can occur for $\mathscr{R}_0$ smaller than that), compared to the case for the Logistic recruitment function which was observed for much larger threshold values. Our belief is that this is the effect of the stronger nonlinearity in the Maynard–Smith–Slatkin function. Moreover, as indicated in Fig. 4, for larger $\mathscr{R}_0$ values, the size of the steady state HRBC population is much larger for the logistic model compared to the Ricker model followed by the more nonlinear Maynard–Smith–Slatkin function. Thus, a stronger parasitemia effect and hence $\mathscr{R}_0$ value is required to reach the balance recruitment–destruction point at which the Hopf bifurcation emerges.

We note that the observed limit cycles were not obtained for the linear growth function.

It is worth noting that for all forms of the recruitment functions, there is a maximal steady state merozoite size. The largest possible such steady state merozoite size is $\frac{(1-\sigma)(1+p_0 e_a)}{\beta(1+p_1 e_a)}$, which is independent of the choice of birth rate function used. Note that the term $\frac{(1-\sigma)}{1+p_1 e_a}$, is a recruitment factor into the merozoite differential equation (2.15), for fixed e_a, indicating that the larger this factor, the larger the merozoite population. Additionally, the size of the bound depends on σ, β and the innate immune cell size. Importantly, when $e_a = 0$, this bound is $\frac{(1-\sigma)}{\beta}$, whose size is larger for smaller σ (which we recall is the proportion of the infected red blood cells that differentiate toward the path to gametocytogenesis) and smaller β (where β is the ratio of the contact rates between IRBCs and merozoites and that between HRBCs and merozoites with a value of at most 1). Note that there is nothing exciting about σ being small since σ implies that more merozoites will be available to infect HRBCs meanwhile a larger σ implies that more IRBCs will follow the path toward gametocytogenesis and once successful in producing male and female gametocytes, will render the human infectious to mosquitoes. Nonetheless, the largest reported σ size is 0.01% as discussed in Ref. 29. For β, a value close to 0, means that the contacts between merozoites and HRBC is dominant and less merozoites are lost via absorption by IRBC.

Our model was analyzed in terms of the innate and adaptive immune variables e_i and e_a. By, construction and nondimensionalization e_i is bounded between 0 and 1 meanwhile we had $e_a > 0$. However, we observed that the steady state size of the innate immune cells given by Eq. (4.13) is bounded above. That is, there is a maximal functional operating steady state size for the innate immune cells and this bound is illustrated in (4.14). With data within a specific human, this size can be analyzed in a malaria patient and the specific immune responses simulated. This is currently under investigation.

Further extensions of our work, under investigation, include the incorporation of a multi-strain infection within a human host and questions of how the immune response acts when more than one strain infects a human. The issue of immune response being parasite specific, needs to be investigated, in addition to the full study on the activation and function of the adaptive immune response. Furthermore, the incorporation of control via anti-malarial drugs are also aspects of this project under further investigation.

6.2. *Conclusion*

To conclude, our model analyses produced limit cycles observed for all forms of the nonlinear recruitment HRBC functions at reasonable threshold parameter values which was not observed when the choice of the recruitment function was linear. We believe this is a novel result and may have several biological implications. We

therefore believe that our work sets the stage to be used to quantify maximal adaptive immune responses in humans and children living in endemic regions. We note that this will require that data be collected from individuals from various age groups and endemic regions since acquired (adaptive) immunity is a function of frequency of exposure to the malaria parasite.

Second, the inclusion of the adaptive immune response, its implicit individual effect captured separately and in conjunction with the innate immune response in inhibiting parasite development has allowed us, perhaps for the first time taking into consideration available published literature, to investigate the effect of the adaptive immune response, which is acquired as a result of repeated exposure to the malaria parasite, on the parasite and hence malaria disease dynamics within a human. We showed that the larger the innate immune size and the better it's efficiency at inhibiting parasite development and progression as discussed in this paper, the less severe the malaria disease is in a malaria patient. A way this was manifested is that the larger the adaptive immune size, the smaller the merozoite and infected red blood cell load which translated to less available free floating merozoites that can infect HRBCs and less IRBCs that can continue the merozoite cyclical path or the path to gametocytogenesis. All these are desirable for reducing the severity and intensity of the malaria infection, as well as the potential size and likely infectiousness and transmissibility of the gametocytes to the mosquitoes. This illustrates, what has been documented, that children who have a poorly developed acquired immunity and visitors to malaria endemic areas with no acquired immunity tend to have a more severe malaria episode than adults living in those endemic areas who have been exposed longer.

Moreover, we believe our model results may shed some light on anecdotal reports/observations that when an individual moves to a new region, he/she typically will have a severe malaria attack. We believe that our model provides a possible answer to this. By our result that shows a negative correlation between innate immune cell size and parasite load and with the suggestion that immune response is parasite specific, when an individual moves to a new region and gets infected, he or she is likely infected with a new parasite strain indigenous to the new region. Since the individual is new to the area, their adaptive immune response to the parasite strain they are newly infected by will be less well defined. Thus, the severity of the malaria attack is probably due to this new strain's impact and effect on destroying the HRBCs, unchecked by adaptive immune response which at this point is not well developed for this specific parasite strain. This requires further investigation but opens up a host of potential questions for biologists and mathematicians alike. One such question is: How is the interaction between a multistage parasite infection and the adaptive immune responses generated due to the presence of the parasite infection(s) with time? With the presence of a well defined adaptive immune response on one parasite, does it enhance the development of the adaptive immune response for the other, if any?

Acknowledgments

WAW, acknowledges support from Lehigh University: the institution, the Mathematics Department and MIT-E's Development fund, for supporting him and hosting him for more than two months as a visiting pre-doctoral scholar, enabling him to make significant progress on the work related to this paper. He also acknowledges support from the African Institute for the Mathematical Sciences (AIMS) Cameroon that paid his flight to visit Lehigh University. All three authors, WAW, MIT-E and GAN acknowledge the support of the NSF -Directorate for Mathematical and Physical Science grant DMS-1544434 that enabled all three to meet during the grant related activities and commence discussions on this paper and related project. MIT-E also acknowledges the sponsorship of the Commission for Developing Countries (CDC) in conjunction with the International Mathematics Union (IMU) through the CDC-ADMP (African Diaspora Mathematicians Program) grant that enabled her collaboration with WAW and GAN during the 2018 grant sponsored visit to the University of Buea. She also acknowledges support via NSF grant 1815912 which enabled her engagement in completing the project. GAN acknowledges the grants and support of the Cameroon Ministry of Higher Education through the initiative for the modernization of research in Cameroon's Higher Education.

References

1. WHO, World malaria report 2018, World Health Organization Bulletin, 2018, https://www.who.int/malaria/publications/world-malaria-report-2018/en/.
2. Hawass Z *et al.*, Ancestry and pathology in king tutankhamun's family, *J Am Med Assoc* **303**(7):638–647, 2010, arXiv:/data/journals/jama/4500/joc05008_638_647. pdf, doi:10.1001/jama.2010.121, http://dx.doi.org/10.1001/jama.2010.121.
3. Cowman AF, Healer J, Marapana D, Marsh K, Malaria: Biology and disease, *Cell* **167**(3):610–624, 2016.
4. Drakeley C, Sutherland C, Bousema TJ, Sauerwein RW, Targett GA, The epidemiology of plasmodium falciparum gametocytes: Weapons of mass dispersion, *Trends Parasitol* **22**(9):424–430, 2006.
5. Gazzinelli RT, Kalantari P, Fitzgerald KA, Golenbock D, Innate sensing of malaria parasites, *Nat Rev Immunol* **14**:744–757, 2014.
6. Langhorne J, *Immunology and Immunopathogenesis of Malaria*, Current Topics in Microbiology and Immunology, Springer, Berlin, Heidelberg, 2006, https://books.google.cm/books?id=tloyrIGdNQgC.
7. Teboh-Ewungkem MI, Ngwa GA, Ngonghala CN, Models and proposals for malaria: A review, *Math Popul Stud* **20**(2):57–81, 2013.
8. Baton LA, Ranford-Cartwright LC, Spreading the seeds of million-murdering death: Metamorphoses of malaria in the mosquito, *Trends Parasitol* **21**(12):573–580, 2005.
9. Teboh-Ewungkem MI, Wang M, Male fecundity and optimal gametocyte sex ratios for plasmodium falciparum during incomplete fertilization, *J Theor Biol* **307**:183–192, 2012.

10. Teboh-Ewungkem MI, Yuster T, A within-vector mathematical model of plasmodium falciparum and implications of incomplete fertilization on optimal gametocyte sex ratio, *J Theor Biol* **264**(2):273–286, 2010.
11. Teboh-Ewungkem MI, Yuster T, Evolutionary implications for the determination of gametocyte sex ratios under fecundity variation for the malaria parasite, *J Theor Biol* **408**:260–273, 2016.
12. Chitnis N, Hyman JM, Cushing JM, Determining important parameters in the spread of malaria through the sensitivity analysis of a mathematical model, *Bull Math Biol* **70**(5):1272–1296, 2008.
13. Ngonghala CN, Teboh-Ewungkem MI, Ngwa GA, Observance of period-doubling bifurcation and chaos in an autonomous ode model for malaria with vector demography, *Theor Ecol* **9**(3):337–351, 2016.
14. Ngonghala CN, Ngwa GA, Teboh-Ewungkem MI, Periodic oscillations and backward bifurcation in a model for the dynamics of malaria transmission, *Math Biosci* **240**(1):45–62, 2012.
15. Ngonghala CN, Teboh-Ewungkem MI, Ngwa GA, Persistent oscillations and backward bifurcation in a malaria model with varying human and mosquito populations: Implications for control, *J Math Biol* **70**(7):1581–1622, 2015.
16. Ngwa GA, Shu WS, A mathematical model for endemic malaria with variable human and mosquito populations, *Math Comput Model* **32**(7):747–763, 2000, https://doi.org/10.1016/S0895-7177(00)00169-2.
17. Teboh-Ewungkem MI, Podder CN, Gumel AB, Mathematical study of the role of gametocytes and an imperfect vaccine on malaria transmission dynamics, *Bull Math Biol* **72**(1):63–93, 2010.
18. Ngwa GA, Niger A, Gumel A, Mathematical assessment of the role of non-linear birth and maturation delay in the population dynamics of the malaria vector, *Appl Math Comput* **217**:3286–3313, 2010.
19. Ngwa GA, On the population dynamics of the malaria vector, *Bull Math Biol* **68**(8):2161–2189, 2006, doi:10.1007/s11538-006-9104-x.
20. Nourridine S, Teboh-Ewungkem MI, Ngwa GA, A mathematical model of the population dynamics of disease transmitting vectors with spatial consideration, *J Biol Dyn* **5**(4):335–365, 2011.
21. Childs LM, Prosper OF, Simulating within-vector generation of the malaria parasite diversity, *PLoS One* **12**(5):e0177941, 2017.
22. Woldegerima WA, Mathematical modeling of the immunopathogenesis of the within human host and the within vector host dynamics of the malaria parasite, Ph.D. thesis, Department of Mathematics, *University of Buea*, Cameroon, 2018.
23. Anderson RM, Complex dynamic behaviours in the interaction between parasite populations and the host's immune system, *Int J Parasitol* **28**(4):551–566, 1998.
24. Antia R, Nowak M, Anderson R, Antigenic variation and the within-host dynamics of parasites, *Proc Natl Acad Sci USA* **93**:985–989, 1996.
25. Chiyaka C, Garira W, Dube S, Modelling immune response and drug therapy in human malaria infection, *Comput Math Meth Med* **9**(2):143–163, 2008.
26. Eckhoff P, *P. falciparum* infection durations and infectiousness are shaped by antigenic variation and innate and adaptive host immunity in a mathematical model, *PLoS One* **7**(9):1–18, 2012, doi:10.1371/journal.pone.0044950, https://doi.org/10.1371/journal.pone.0044950.
27. Johnson P, Kochin B, Ahmed R, Antia R, How do antigenically varying pathogens avoid cross-reactive responses to invariant antigens?, *Proc Biol Sci* **279**(1739):2777–2785, 2012.

28. Tewa J-J, Fokouop R, Mewoli B, Bowong S, Mathematical analysis of a general class of ordinary differential equations coming from within-hosts models of malaria with immune effectors, *Appl Math Comput* **218**(14):7347–7361, 2012.
29. Woldegerima WA, Teboh-Ewungkem MI, Ngwa GA, The impact of recruitment on the dynamics of an immune-suppressed within-human-host model of the Plasmodium falciparum parasite, *Bull Math Biol* **81**:4564–4619, 2019, doi:10.1007/s11538-018-0436-0.
30. Cai L, Tuncer N, Martcheva M, How does within-host dynamics affect population-level dynamics? insights from an immuno-epidemiological model of malaria, *Math Meth Appl Sci* **40**:6424–6450, 2017.
31. Menendez C, Fleming A, Alonso P, Malaria-related anaemia, *Parasitol Today* **16**(11):469–476, 2000.
32. Kaushal D, Carter R, Miller L, Krishna G, Gametocytogenesis by malaria parasites in continuous culture, *Nature* **286**(5772):490–492, 1980.
33. Talman AM, Domarle O, McKenzie FE, Ariey F, Robert V, Gametocytogenesis: The puberty of plasmodium falciparum, *Malaria J* **3**(1):24, 2004.
34. Bousema T, Drakeley C, Epidemiology and infectivity of *Plasmodium falciparum* and *Plasmodium vivax* gametocytes in relation to malaria control and elimination, *Clin Microbiol Rev* **24**(2):377–410, 2011.
35. Cuomo MJ, Noel LB, White DB, Diagnosing medical parasites: A public health officers guide to assisting laboratory and medical officers, Technical Report, DTIC Document, 2009.
36. Eichner M, Diebner HH, Molineaux L, Collins WE, Jeffery GM, Dietz K, Genesis, sequestration and survival of plasmodium falciparum gametocytes: Parameter estimates from fitting a model to malariatherapy data, *Trans Roy Soc Trop Med Hygiene* **95**(5):497–501, 2001.
37. Gardiner DL, Trenholme KR, Plasmodium falciparum gametocytes: Playing hide and seek, *Ann Transl Med* **3**(4):45, 2015, doi:10.3978/j.issn.2305-5839.2015.01.23.
38. Kiszewski AE, Blocking plasmodium falciparum malaria transmission with drugs: The gametocytocidal and sporontocidal properties of current and prospective antimalarials, *Pharmaceuticals* **4**(1):44–68, 2010.
39. Kuehn A, Pradel G, The coming-out of malaria gametocytes, *J Biomed Biotechnol* **2010**:976827, 2010, doi:10.1155/2010/976827.
40. Perlmann P, Troye-Blomberg M, *Malaria Immunology, Chemical Immunology and Allergy*, Karger, 2002, https://books.google.cm/books?id=dSVWAQAAQBAJ.
41. Li Y, Ruan S, Xiao D, The within-host dynamics of malaria infection with immune response, *Math Biosci Eng* **8**(4):999–1018, 2011.
42. Woldegerima WA, Ngwa GA, Teboh-Ewungkem MI, Sensitivity analysis for a within-human host immuno-pathogenesis dynamics of Plasmodium falciparum parasites, in *Mathematical Methods and Models in Biosciences*, Anguelov R, Lachowicz M (eds.), Sofia, pp. 140–168, 2018, http://dx.doi.org/10.11145/texts.2018.05.257.
43. Hetzel C, Anderson R, The within-host cellular dynamics of bloodstage malaria: Theoretical and experimental studies, *Parasitology* **113**(1):25–38, 1996.
44. Garnham P, *Malaria Parasites and Other Haemosporidia*, Blackwell Scientific Publications, 1966.
45. Anderson R, May R, Gupta S, Non-linear phenomena in host parasite interactions, *Parasitology* **99**(S1):S59–S79, 1989.
46. Okrinya A, Mathematical modelling of malaria transmission and pathogenesis, Ph.D. thesis, Loughborough University, 2015.

47. De Leenheer P, Within-host virus models with periodic antiviral therapy, *Bull Math Biol* **71**(1):189–210, 2009.
48. Iggidr A, Kamgang J-C, Sallet G, Tewa J-J, Global analysis of new malaria intrahost models with a competitive exclusion principle, *SIAM J Appl Math* **67**(1):260–278, 2006.
49. Brännström Å, Sumpter D, The role of competition and clustering in population dynamics, *Proc Roy Soc B* **272**:2065–2072, 2005.
50. Tetschke M, Lilienthal P, Pottgiesser T, Fischer T, Schalk E, Sager S, Mathematical modeling of rbc count dynamics after blood loss, *Processes* **6**(9), 2018, doi:10.3390/pr6090157, https://www.mdpi.com/2227-9717/6/9/157.
51. Verhulst PF, Notice sur la loi que la population suit dans son acroissement, *Corres Math Phys* **10**:113–121, 1838.
52. Pearl R, *The Biology of Population Growth*, Alfred A. Knopf, New York, 1925.
53. Ricker WE, Stock and Recruitment, *J Fisher Res Board Canada* **11**:559–623, 1954.
54. Nisbet RM, Gurney W, *Modelling Fluctuating Populations*, John Wiley & Sons, 1982.
55. Maynard-Smith J, Slatkin M, The stability of predator–prey systems, *Ecology* **54**:384–391, 1973.
56. Beverton RJH, Holt SJ, *On The Dynamics of Exploited Fish Populations*, Fisheries Investment Vol. 2, Her Majesty Stationary Office, London, 1981.
57. Van den Driessche P, Watmough J, Reproduction numbers and sub-threshold endemic equilibria for compartmental models of disease transmission, *Math Biosci* **180**(1):29–48, 2002.
58. Kotepui M, Piwkham D, PhunPhuech B, Phiwklam N, Chupeerach C, Duangmano S, Effects of malaria parasite density on blood cell parameters, *PLoS One* **10**(3):e0121057, 2015.
59. Mideo N, Day T, Read A, Modelling malaria pathogenesis, *Cell Microbiol* **10**(10):1947–1955, 2008.